Stony Brook University

Layer and Cell Type Specific Functional Properties of Gustatory Cortex Neurons

A Dissertation Presented

by

Gulce Nazli Dikecligil

to

The Graduate School

in Partial Fulfillment of the

Requirements

for the Degree of

Doctor of Philosophy

in

Neuroscience

Stony Brook University

August 2017

Stony Brook University

The Graduate School

Gulce Nazli Dikecligil

We, the dissertation committee for the above candidate for the

Doctor of Philosophy degree, hereby recommend

acceptance of this dissertation.

Alfredo Fontanini
Associate Professor Department of Neurobiology and Behavior

Giancarlo La Camera
Associate Professor Department of Neurobiology and Behavior

Lorna Role
SUNY Distinguished Professor and Chair Department of Neurobiology and Behavior

Steve Shea
Associate Professor Cold Spring Harbor Laboratory

Mark Laubach
Associate Professor of Biology American University

This dissertation is accepted by the Graduate School

Charles Taber

Dean of the Graduate School

Abstract of the Dissertation

Layer and Cell Type Specific Functional Properties of Gustatory Cortex Neurons

by

Gulce Nazli Dikecligil

Doctor of Philosophy

in

Neuroscience

Stony Brook University

2017

The primary gustatory cortex is the cortical region devoted to processing taste. The gustatory cortex receives a wide range of projections from brain regions involved in sensory, limbic and cognitive functions. The functional properties of gustatory cortical neurons reflect this complex anatomical connectivity, encoding taste, sensorimotor, hedonic and anticipatory components of taste stimuli. No study to date has addressed whether there are differences in the functional properties of cortical neurons belonging to distinct layers and cell types.

To address this question, I have performed a series of experiments using tract tracing and extracellular electrophysiological methods in mice.

I demonstrate that in licking animals, firing rates of gustatory cortex neurons are modulated prior to the arrival of taste stimuli and this pre-stimulus modulation is biased to deep layer inhibitory neurons. Furthermore, I show that neurons in deep and superficial layers have distinct firing rates at baseline and stimulus evoked epochs. In the stimulus-evoked period, licking activity structures the activity of gustatory cortex where a subset of pyramidal neurons shows precise action potential timing within the lick cycles. Finally, I show that neurons that display pre-stimulus modulations and licking rhythm dependent activity can encode taste information. Together, the work presented in this dissertation provides fundamental insights into the distinct functional properties of gustatory cortex neurons belonging to distinct lamina and cell types.

Table of Contents

Chapters

Table of Figures

CHAPTER 1

Introduction

The cerebral cortex is composed of many cytoarchitecturally distinct, functionally specialized, but highly interconnected regions that are responsible for processing information related to sensory, motor, and cognitive functions [1, 2]. Within the cerebral cortex, primary sensory cortices perform computations pertaining to stimuli from their corresponding sensory modality. These regions play a crucial role in extracting complex features of sensory stimuli arriving from the ascending sensory pathways. The ability of the primary sensory cortices to act as a node that integrates bottom up sensory inputs with top down contextual information is critical in endowing animals with the ability to interpret and respond to external stimuli in an adaptive, context dependent manner.

Accumulating evidence from experimental and theoretical studies suggest that the complex functions of primary sensory cortices can be attributed to the connectivity pattern of their constituent neurons [2, 3]. A key organizational principle of sensory cortices is their laminar structure, where neurons belonging to a given layer are densely packed and spatially segregated from neurons located in other layers. This laminar organization is not purely an anatomical feature, but also structures the functional relationship of cortical neurons. Neurons in different layers receive different inputs and connect to one another with specific probabilities and strengths shaping the information flow in cortical circuits [1]. In addition to the laminar structure, the relationship between different cell types, in particular the excitatory and inhibitory cell types, is a key factor in shaping cortical processing. Overall, these findings have suggested that cortical circuits have organizational themes that partially dictate the functional properties of individual cortical neurons.

While a great deal of work has been done to understand the differences in functional properties of neurons belonging to different lamina and cell types in visual, auditory, somatosensory and to some extent in olfactory cortices [4-17], there has been no studies addressing the functional properties of gustatory cortical neurons in a lamina and cell type specific manner. The dissertation work presented here aims to bridge this gap.

The gustatory cortex is the primary sensory cortex devoted to processing taste information. Positioned within the insular cortex on the lateral surface of the rodent's brain, the gustatory cortex receives taste related information from the ascending gustatory pathway. Studies

in anesthetized and awake rodents have revealed that gustatory cortex neurons can respond to taste as well as tactile, olfactory and visceral stimuli [18-21]. Furthermore, it has been shown that gustatory cortex neurons respond to cues that predict taste delivery [21-23]. Interestingly, the responses of gustatory cortex neurons can change with learning, suggesting that representations of taste and other sensory stimuli in gustatory cortex are not fixed [21, 24, 25].

While the response properties of gustatory cortex neurons have previously been investigated, a systematic study of the functional properties of neurons belonging to distinct lamina and cell types has not been undertaken yet. To address this gap in the literature, I have performed a series of experiments aimed at understanding how neurons belonging to different lamina and cell types (i.e. excitatory and inhibitory) encode chemosensory, somatosensory and anticipatory features of taste related activity.

In Chapter I of my thesis, I will first discuss the findings from other primary sensory cortices, focusing on the connectivity and functional properties of neurons belonging to different lamina and cell types. I will highlight the general organizational principles that apply to primary sensory cortices and when applicable discuss how the functional properties arise from the underlying cortical circuitry. Next, I will introduce the anatomy of the gustatory system beginning at the periphery and moving up the ascending taste pathway to the gustatory cortex. I will briefly discuss the functional properties of neurons throughout the gustatory pathway before focusing on the organization and functional properties of the gustatory cortex. The functional properties of gustatory cortex neurons will be discussed in terms of taste coding as well as their properties beyond taste coding. The last section of this chapter will present the rationale for the work presented in here and outline the contents of the dissertation.

1.1. Layer and Cell Type Specific Sensory Coding in Primary Sensory Cortices

1.1.1. Organizational Principles of Neurons within Primary Sensory Cortices

Primary sensory cortical areas receive information from ascending pathways corresponding to their sensory modality and process complex features of sensory stimuli. With the exception of the olfactory system, sensory input into the cortex is relayed from dedicated sensory thalamic nuclei. As summarized in Figure 1A, in areas with a six-layer laminar organization, namely the primary visual cortex, the somatosensory cortex and the auditory cortex, projections from sensory thalamic nuclei mainly target L4 and L6 [26, 27]. This sensory thalamic input is integrated with projections from other higher order cortical and thalamic regions which project mainly to neurons in L1, L5 and L6 [28]. Within a given primary sensory cortical region, L4 neurons are the main recipient of sensory thalamic input. Neurons in L4 project most densely to L2/3 neurons, which in turn send their projections to higher order cortical

areas, contralateral cortices and to L5 neurons. Within the local cortical circuit, L5 neurons receive inputs from all other layers and project strongly to long-distance targets, broadcasting the integrated information. L6 is composed of neurons that communicate predominantly with other local cortical neurons as well as a second group of neurons who integrate inputs from higher order cortical regions and in return send feedback to sensory and reticular thalamic nuclei.

Each primary sensory cortex is composed of neurons with distinct properties distributed throughout its layers. This heterogeneous population of neurons can be classified according to a variety of their diverse features, including the neurons' gene expression profiles, morphological features, physiological properties and connectivity patterns. The best understood and the most functionally informative classification is the distinction between excitatory and inhibitory neurons. I will review these two categories of neurons in terms of their anatomical and functional properties. Each category will be further divided into subcategories where excitatory neurons will be classified according to their connectivity patterns, and inhibitory interneurons will be classified based on their genetic markers.

Excitatory neurons

Excitatory neurons can be found in all layers of the cortex and make up about 80% of the cortical neuron population. These neurons release the neurotransmitter glutamate which binds to the fast acting, ligand gated ion channels (AMPA and NMDA) and/or slow acting metabotropic receptors (mGluRs) on the post-synaptic site leading to depolarization. Excitatory neurons can form both local and long-range synaptic connections with other excitatory and inhibitory neurons. The anatomical location of the post-synaptic target has been one of the main features used to further classify excitatory neurons into subcategories.

Intratelencephalic neurons

The first category of excitatory neurons is the Intratelencephalic (IT) neurons located in L2 through L6. IT neurons only project to other areas within the telencephalon (striatum, neocortex, amygdala and claustrum). A key feature that separates IT neurons from the rest of excitatory neuron subcategories is that a proportion of neurons within this category project to the contralateral cortex via the corpus callosum and the anterior commissure [1]. The subset of IT neurons that only project to other cortical neurons are called corticocortical neurons (CC). As IT is composed of neurons with very diverse input-output connectivity patterns and physiological response properties, the functional role of IT neurons is not homogenous and cannot be generalized across neurons belonging to different lamina within the category [1, 2].

Cortico-thalamic neurons

The next category of excitatory neurons is the corticothalamic neurons (CT). The neurons in this category are located in L6 and are characterized by their axonal projections to thalamic nuclei. Within thalamus, CT neurons project to the reticular nucleus and to the thalamic nuclei corresponding to their sensory modality. This cortical feedback has complex effects on the

sensory thalamic nuclei; the reticular nucleus is primarily composed of inhibitory neurons and projects to the sensory thalamic nuclei thus providing disynaptic inhibition. Due to this complexity, the net effect of CT feedback on sensory processing in thalamus is not fully understood. However, a recent study in the somatosensory system investigated the functional role of L6 CT neuron stimulation on thalamic neurons. The authors used optogenetic stimulation of the CT neurons of barrel cortex in anesthetized mice and intracellularly recording from the neurons in VPM. The authors reported that the CT stimulation reduced the adaptation of thalamic neurons to repetitive whisker stimulation and allowed for relay of higher frequency sensory input to the cortex [29].

CT neurons are a major output of primary sensory cortices playing a crucial role in providing feedback onto the thalamic neurons. In experiments combining whole cell patch clamp recordings in the primary visual cortex of mice with single-cell retrograde trans-synaptic tracing, Velez-Fort et al. have shown that, CT neurons, in contrast to the corticocortical (CC) neurons located in the same layer (L6), receive much denser synaptic input from higher order areas and much smaller density of projections from neurons within the local cortical circuit. In addition, CT neurons display narrow tuning properties to orientation and direction unlike the CC neurons which display broad tuning in their spiking and subthreshold responses. Interestingly, it has been shown that in awake mice, CT neurons in primary visual cortex fire very sparsely during visual stimulation [30] and it remains to be seen whether such sparse activity can nonetheless induce meaningful changes in thalamic sensory processing as reported in [29].

Taken together, these findings suggest that the narrowly tuned CT neurons can provide stimulus specific feedback onto thalamic neurons. While the exact mechanisms of how the CT neurons influence thalamic activity and the possible range of CT's influence in thalamocortical interaction is unclear, it is evident that they could alter the mode of communication in the thalamocortical loops in a state and context dependent manner.

Subcerebral Neurons

The last class of excitatory neurons is the subcerebral projection neurons (SPN), which are considered to be one of the final outputs cortical excitatory circuit. SPNs receive input from all layers of the local cortical circuit as well as from thalamic nuclei. Due to this input pattern, SPNs are thought to integrate cortical and thalamic information and send the resulting information to distant subcortical targets. The subcortical target of SPNs depends on which cortical area the SPNs are located in. For example, the SPNs of primary visual cortex project to the superior colliculus [2], while the SPNs of barrel cortex project to the spinal trigeminal nuclei to promote whisker retraction [31]. SPNs also form the well-studied pyramidal tract of the primary motor cortex, sending direct projections to the spinal cord [32]. In addition to broadcasting to subcerebral regions such as the midbrain, brainstem and the spinal cord, the axon collaterals of SPNs also project to ipsilateral cortex, thalamus and striatum.

Inhibitory neurons

Inhibitory interneurons, which only project to local neurons within a given cortical region, constitute 20% of the neurons in the cortex and release the neurotransmitter GABA. The binding of GABA to the fast acting ionotropic ($GABA_A$) and/or slow acting metabotropic receptors ($GABA_B$) leads to a suppressive effect on the post-synaptic neuron either through hyperpolarization or through shunting inhibition. Aside from the common feature of releasing GABA, cortical inhibitory neurons are very diverse in their morphology, gene expression profiles, molecular markers, ion channel compositions, physiological properties, and where they synapse on at the post-synaptic target. Given this great diversity of features, the taxonomy of cortical inhibitory neurons has attracted a lot of attention [33-35]. With the recent developments in mouse genetic tools, classifying inhibitory neurons according to their gene expression profile has been the dominant method for studying their properties and function. According to this criterion, there are three main categories of non-overlapping, genetically tractable inhibitory neurons: the parvalbumin expressing interneurons (PV), somatostatin-expressing interneurons (SOM) and 5HT3A-receptor expressing interneurons (including vasoactive intestinal peptide expressing, VIP neurons).

PV neurons, which are characterized by high firing rates, are composed of two main subgroups of morphologically distinct neurons: the basket cells and the chandelier cells [34]. PV cells receive inputs from other inhibitory neurons, sensory thalamus, and cortical excitatory neurons. In return PV cells project to the soma (basket cells), or axon initial segment (chandelier cells) of the local excitatory neurons. This projection pattern positions PV cells in a crucial place to alter the synaptic integration of inputs at the soma or the final output of the neuron at the axon initial segment [1]. SOM neurons are mainly composed of Martinotti cells which target the distal dendrites of excitatory neurons. The main input onto SOM neurons comes from local excitatory neurons and VIP neurons. The final category of inhibitory neurons is the 5HT3A category, mainly composed of VIP and Neurogliaform type (NG) neurons [2]. While the PV and SOM neurons are distributed across all layers, VIP neurons are predominantly located in the superficial layers of cortex. VIP neurons preferentially target SOM neurons and are thought to play a critical role in regulation of inhibition in primary sensory cortical regions [9]. Figure 1B summarizes the interconnectivity among inhibitory neurons and their projections onto pyramidal cells.

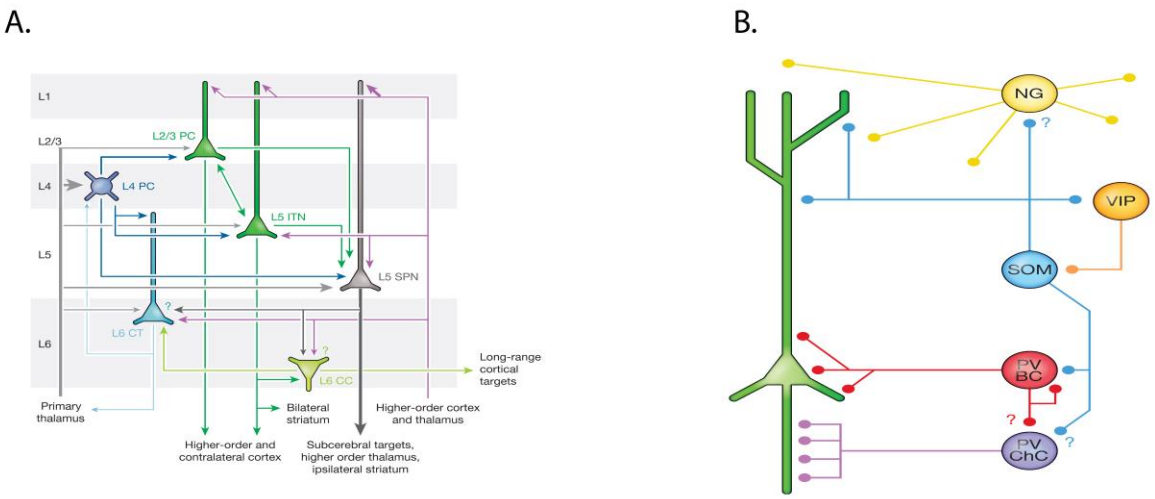

Figure 1. Cortical Connectivity

A. Connectivity pattern among the principal cells of six layered neocortical regions. The schematic illustrates the main inputs onto the different cortical layers and the main outputs from each layer. The thickness of the lines indicates the strength of the connection between two regions. Primary sensory thalamus primarily targets L4. Higher order input from cortex and non-sensory thalamic nuclei target L2/3 and L5 neurons. Corticocortical outputs mainly arise from the L2/3 and L6 neurons whereas outputs to subcerebral regions arise from L5 neurons. Cortical feedback onto the thalamic nuclei arises exclusively form L6 neurons.

B. Connectivity pattern among excitatory and genetically identified interneuron subtypes. Pyramidal neuron (in green) receives inhibitory input from both PV and SOM interneurons. VIP neurons can inhibit SOM neurons leading to disinhibition of pyramidal neurons.
Panels are taken and adapted from [1]

1.1.2. Sensory Responses in Primary Sensory Cortices

Laminar differences in sensory processing

Neurons in primary sensory cortices can respond to specific features of sensory stimuli such as orientation of a visual stimulus, the frequency of an auditory tone or chemical composition of an olfactory stimulus. The range of stimuli that elicit suprathreshold responses determines the neuron's breadth of tuning. For example, a V1 neuron responding to bars with varying orientations would be a broadly tuned neuron, whereas a neuron responding only to bars with a specific orientation would be narrowly tuned. Breadth of tuning is a widely studied property as it informs us about how different sensory stimuli are represented at the single neuron level. After having discussed the connectivity in the previous section, I will next discuss the responses of primary sensory cortical neurons to sensory stimuli.

With advances in electrophysiological methods that allow for simultaneous, multi-channel recordings across distinct layers of cortex, the field has seen an increase in the number of studies looking at the activity pattern of neurons in primary sensory cortices across layers. The use of optogenetics has further enhanced the ability to record from different cell types and study their properties in awake animals. These studies have elucidated spontaneous and stimulus evoked firing rate patterns of neurons belonging to distinct categories and begun to unveil the principles of sensory coding.

In one of the first studies to investigate response properties across layers of primary sensory cortices in awake rodents, Krupa et. al., demonstrated layer-dependent firing rate profiles in somatosensory cortex (S1) during a whisker based discrimination task. Both the strength and the duration of stimulus evoked responses were distinct across L2/3, L4, and L5/6. Neurons in deep and superficial layers responded with long lasting firing rate modulations, with deep layers showing stronger modulations compared to the superficial layers. In contrast, L4 neurons displayed weaker and shorter lasting firing rate modulations compared to L2/3 and L5/6. While a variety of response profiles were observed (i.e. purely excitatory, purely inhibitory or a mixed pattern) across all layers, the prevalence of these response patterns showed layer specificity; for example, L4 neurons were more likely to display mixed response pattern where stimulus evoked inhibition was followed by excitation. Most importantly, ensembles of deep layer neurons could discriminate stimulus identity more accurately compared to ensembles of superficial layer neurons [36]. This layer dependency of sensory coding in somatosensory cortex was replicated in a similar study where single neurons from L4 and L5 showed higher stimulus discrimination performance compared to single neurons from L2/3 [17]. It is important to note that while L2/3 did contain neurons that were highly discriminative across stimulus features, the overall percentage of such neurons was much lower compared to that of L4 and L5.

Layer dependence of stimulus evoked firing rate patterns and sensory coding properties were observed in other primary sensory cortices across different studies [6, 37, 38]. As shown in Figure 2B, in a study investigating spontaneous and evoked response properties in auditory cortex, L2/3 neurons showed much lower firing rates compared to L4/5 in both conditions.

Furthermore, thalamorecipient layers showed earlier response onset compared to non-thalamorecipient layers, consistent with a feedforward processing model [39]. For both cortical regions, the authors attributed the observed differences to the distinct connectivity pattern of each layer. In Krupa et al., the authors reasoned that the long response duration in deep and superficial layers were related to the disproportionate intracortical and top-down input these layers received compared to the thalamorecipient L4. In Sakata et., al, the authors suggested that the consistency of sparse firing activity in L2/3 neurons across spontaneous and sensory evoked conditions was an indication of the underlying circuit properties where L2/3 neurons received disproportionate inhibitory drive compared to neurons in deeper layers. Support for this hypothesis came from a later study where the authors used whole cell patch clamp to isolate the inhibitory and excitatory inputs onto L2/3 neurons in the somatosensory cortex. They found that when mice were actively whisking the neurons in L2/3 fired very few spikes, and this was due to inhibitory inputs being stronger than excitatory inputs during active whisking [13].

A recent study in the mouse visual cortex [30] has provided further evidence supporting the idea that the functional properties of neurons are a reflection of their inputs. This study demonstrated that in L6 of visual cortex, there were at least two functionally distinct response patterns: sparse and selective versus dense and broadly tuned responses. Interestingly these two functional categories mapped onto two distinct subpopulations of neurons in L6, the corticothalamic neurons and the corticocortical neurons respectively. These two subcategories of L6 neurons were shown not only to be distinct in their projection targets but also to be different in their input patterns demonstrating the role of connectivity patterns in determining the functional properties of cortical neurons.

Overall, these studies show that neurons across different layers of primary sensory cortices display distinct firing rate profiles during spontaneous and stimulus evoked epochs, which reflect their distinct connectivity patterns within the cortical circuits. At the moment, it is unclear whether the relative differences observed across layers of a given primary sensory area would be conserved for a different primary sensory cortical area.

Differences in sensory processing between excitatory and inhibitory neurons

Interactions among excitatory and inhibitory neurons, along with the interactions across layers, shape cortical computations [1, 2, 40]. While both excitatory and inhibitory neurons receive synaptic inputs from long range projections, such as thalamus, amygdala and associative cortices [12, 21, 22], a significant portion of their inputs arise from other excitatory and inhibitory neurons within the local cortical circuit. It is important to note that while interdependent, the relative timing and strength of the two populations' activity is not fixed and can change in a context and stimulus dependent manner. This flexibility in how the two populations interact allows for a wide range of cortical dynamics increasing the capacity for information processing. Below I will review the functional properties of excitatory and inhibitory neurons in primary sensory cortices and discuss how their interactions contribute to sensory processing.

One of the best studied properties of neurons in primary sensory cortices is their tuning properties. Calcium imaging in mouse visual cortex has revealed that excitatory neurons respond

to a selected range of orientations (narrowly tuned), whereas inhibitory neurons respond to a broader range of orientations. This difference in the tuning properties of excitatory and inhibitory neurons was observed across different primary sensory cortices of mice suggesting that it might be a common sensory processing feature [6, 41-45].

How do these differences in breadth of tuning arise? Similar to the differences in functional properties of neurons belonging to distinct lamina, it is thought that the functional differences of excitatory and inhibitory neurons also arise from their distinct upstream connectivity [1, 40]. In the mouse visual cortex it has been shown that inhibitory neurons non-selectively receive inputs from local neurons with diverse preferred orientations, whereas pyramidal neurons receive inputs from other pyramidal neurons with similar preferred orientations [46-49]. This functional heterogeneity in the upstream neurons is thought to endow inhibitory neurons with broader tuning compared to the pyramidal neurons. Further support for this hypothesis comes from studies in areas where there is a clear sensory map (i.e. neurons with similar functional properties are clustered together). In this case, inhibitory neurons, connected non-selectively to nearby excitatory neurons, display narrow tuning properties [50]. These findings suggest that the tuning properties of inhibitory neurons depends on the degree of functional heterogeneity in the local pyramidal neurons; in sensory areas where all local pyramidal neurons are tuned to the same sensory features (ex, cat visual cortex), the inhibitory neurons display narrow tuning whereas in sensory areas in which the functional properties of nearby neurons are dissimilar (ex, mouse visual cortex), the inhibitory neurons display broadly tuned responses.

How do the interactions between inhibitory and excitatory neurons shape cortical computations? It has been shown that the relative timing and strength of excitatory and inhibitory currents in cortical circuits change in a stimulus and context dependent manner, suggesting that this interaction plays an important role in sculpting cortical computations.

In visual, auditory and somatosensory cortical neurons, brief sensory stimuli lead to excitatory responses that are followed by inhibition [8, 51, 52]. It is hypothesized that this specific temporal relationship between the excitatory and inhibitory currents determines the temporal window within which the neuron can respond to a sensory stimulus ultimately controlling the duration of the stimulus response. Furthermore evidence shows that this temporal window can change in a stimulus specific manner where non-preferred stimuli evoke rapid inhibition, shortening the coding window, and preferred stimuli evoke late inhibition, lengthening the coding window [52]. This temporal relationship between the two conductances is poised to shape the timing, duration and breadth of tuning of a neuron's responses to sensory stimuli.

An important factor that affects a neuron's sensory responses is the relative strength of the excitatory versus inhibitory inputs it receives across different sensory stimuli. Early studies using pharmacological methods have shown that application of $GABA_A$ antagonists leads to broader tuning curves for excitatory neurons, suggesting that inhibition plays an important role in shaping response selectivity [4, 53-55]. Follow-up experiments investigating the mechanisms through which inhibition contributes to stimulus selectivity revealed that neurons receive both strong excitation and strong inhibition in response to their preferred stimuli [8, 43, 52, 56]. This

finding has challenged the former theories positing that stimulus selectivity arises as a result of preferred stimuli eliciting strong excitation coupled by weak inhibition. In light of these findings, the current theories propose that inhibition sharpens tuning curves by amplifying the contrast between the responses to preferred versus the non-preferred stimuli. It is thought to do so by keeping the weak excitatory inputs elicited by non-preferred stimuli below threshold.

Overall the findings summarized in this section illustrate that the relationship between excitatory and inhibitory neurons in primary sensory cortices shapes sensory processing through changes in their relative timing and strength.

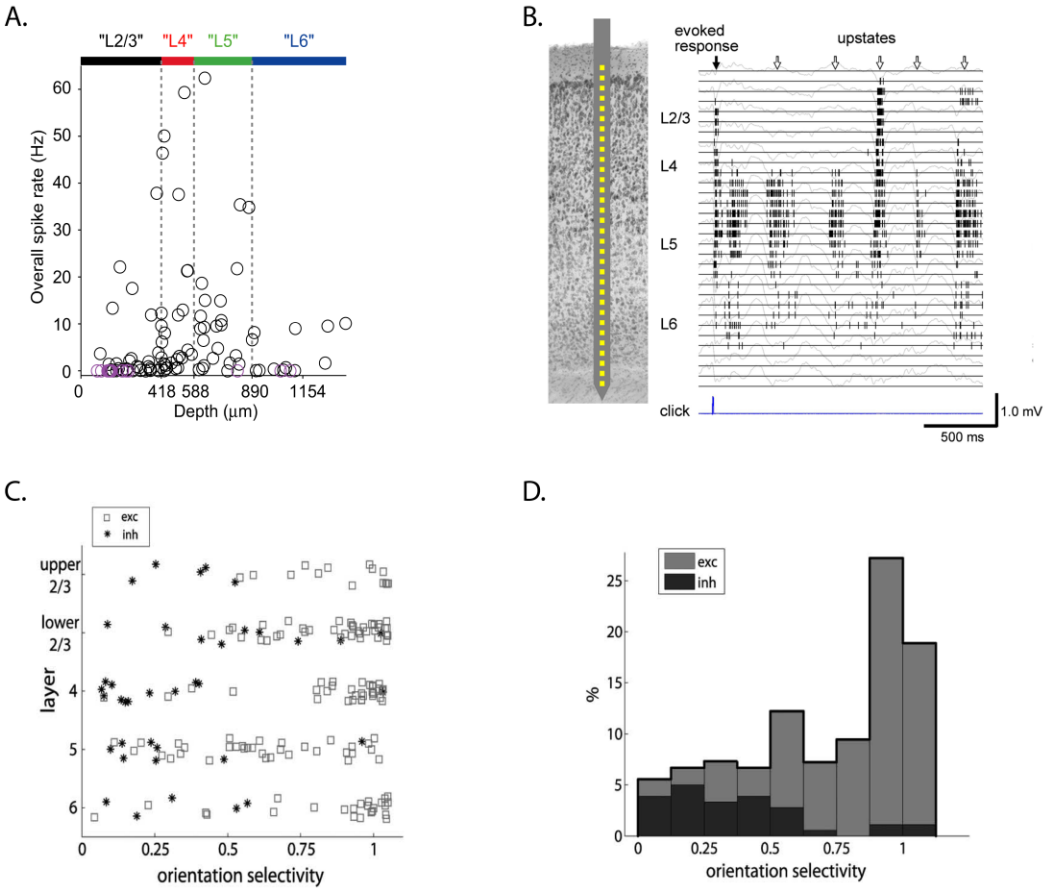

Figure 2. Laminar and Cell Type Specific Properties

A. Average firing rate of barrel cortex neurons distributed across layers in awake mice performing a whisker based object localization task. Each circle represents a single, juxtacellularly recorded neuron. Purple circles indicate neurons that did not fire throughout the recording session. Neurons with high firing rates are more likely to be located in L4-L5 while L2/3 neurons predominantly display low firing rates. Panel adapted from [17].

B. Simultaneously recorded action potentials across layers of auditory cortex in anesthetized rats. Auditory-evoked and spontaneous firing rate profiles of neurons differ across layers

with L2/3 and L6 neurons showing lower firing rates compared to L4-L5. Panel adapted from [57].

C. Orientation selectivity of visual cortex neurons in anesthetized mice. Each square represents a putative excitatory neuron and each star represents a putative inhibitory neuron. The orientation selectivity ranges from 0 to 1 where 0 indicates that neuron responds in the same way to all orientations (broad tuning) whereas a value of 1 indicates perfect selectivity (narrow tuning) with the neuron only responding to a single orientation. A greater percentage of neurons in L2/3 display narrowly tuned responses. Panel adapted from [58].

D. Orientation selectivity of putative excitatory and putative inhibitory neurons in visual cortex neurons in anesthetized mice. Neurons from all layers are pooled together. Inhibitory neurons are more broadly tuned compared to excitatory neurons. Adapted from [58].

1.1.3. Beyond sensory coding in primary sensory cortices

In this section, I will discuss experimental findings that illustrate how neural activity in primary sensory cortices can be shaped by cross-modal stimuli and by the behavioral state of the animal. When possible, I will point to the putative mechanisms underlying the observed effects and discuss the functional implications of these modulations.

The majority of studies investigating response properties of neurons in primary sensory cortices have used unimodal stimuli. Recent years have seen an increase in experiments using cross-modal stimuli to assess how primary sensory cortices respond to stimuli in other modalities. These studies have shown that visual cortex can be modulated by auditory stimuli [59], and auditory cortex can respond to both visual and somatosensory stimuli [60, 61]. These cross-modal representations have also been observed in the chemical senses where both piriform and gustatory cortices respond to stimuli in the other sensory modality [19, 62, 63]. Overall, these studies have revealed that contrary to a segregated view of sensory processing, all primary sensory cortices are modulated by cross-modal stimuli. The role of these cross-modal responses and how they shape sensory processing in a given cortical region is an active area of research.

The presentation of unimodal or cross-modal stimuli does not elicit fixed responses in primary sensory cortices. Stimulus evoked responses change depending on the brain state, as assessed by local field potential (LFP) recordings. Changes in brain state are the most evident in sleep/wake cycles as LFP signals go from synchronized, slow oscillations to desynchronized activity. However, changes in brain states are not limited to sleep/wake cycles, as they can be induced by many behavioral, cognitive or internal signals [64-66]. While the pathways promoting these state changes have not been fully elucidated, many studies point to the role of thalamocortical and neuromodulatory projections in driving cortical state changes [15, 67-71].

State changes influence sensory processing. In an elegant series of experiments, Petersen and colleagues have shown that whisking versus quiet wakeful states give rise to distinct activity patterns in somatosensory cortex that can be observed at both population and single neuron level [72]. During quiet wakefulness, LFPs in barrel cortex displayed slow oscillations and these slow oscillations markedly reduced when animals started whisking. These differences in brain state had important implications for sensory processing, as whisker stimulation during active states induced much smaller post-synaptic potentials compared to whisker stimulation during quiet wakeful states [15]. In fact, this dependence of sensory responses on ongoing brain states has been shown across many sensory cortices [7, 65, 73-77].

In the primary auditory cortex of mice, state changes induced by locomotion specifically affected the sensory evoked responses of L2/3 neurons and L4 responses were unchanged. The authors also observed that thalamic responses were unaltered across the different behavioral states, suggesting that the effects were either due to layer specific corticocortical inputs or neuromodulatory projections. These results show that not only do behavioral states influence brain states and alter sensory processing, but they can do so in a layer specific fashion [75].

All in all, these results demonstrate that primary sensory cortices can respond to stimuli beyond their corresponding sensory modality and the stimulus evoked responses can be

modulated by behavioral states and context. This state dependency of cortical responses is thought to arise from a combination of corticocortical, thalamocortical and neuromodulatory inputs, allowing primary sensory cortices to process bottom-up sensory inputs in context of the animals' internal and external conditions.

1.2. Anatomical and Synaptic Organization of Gustatory System

The findings summarized above demonstrate that different cell types in different layers have distinct upstream connectivity patterns that ultimately shape their functional properties. These distinct functional properties underlie cortical computations and sensory processing. While studies in visual, auditory, somatosensory and partially in olfactory cortices begun to elucidate the functional distinctions across their constituent neurons, such an understanding is lacking in the primary gustatory cortex. In the sections below, I will discuss our current understanding of the gustatory pathway and the role of gustatory cortex within this system and finish by summarizing the diverse functional properties of gustatory cortex neurons in awake rodents.

1.2.1. Ascending Taste Pathway to the Gustatory Cortex

The gustatory system processes information related to food and beverages, guiding animals' consummatory behaviors. It does so by detecting the chemical content of foods and integrating it with its other diverse features such as texture and temperature using the inputs provided by other sensory systems.

The gustatory system of mammals can detect five different chemical groups; sugars, salts, acids, alkaloids and amino acids ultimately leading to the perception of sweet, salty, sour, bitter and umami respectively. Taste detection begins by binding of chemicals to the corresponding taste receptors found on taste receptor cells (TRC). Each TRC expresses a single receptor type that can detect a single taste quality. TRCs are located into taste buds that are distributed throughout the tongue and the oral cavity. Each taste bud contains up to 100 TRC, each expressing different taste receptors. This grouping of diverse TRCs allows for possible cross talk via the release and binding of neurotransmitters (e.g., serotonin) at the level of the taste buds. The extent of this crosstalk and how it influences TRC responses at the periphery is an active area of research [78, 79].

Three different cranial nerves; the chorda tympani, the superior petrosal and the glossopharyngeal nerves, innervate the oral region and carry information from the taste receptor cells to the nucleus of the solitary tract (NTS) in the brain stem. Electrophysiological recordings in the NTS of awake and anesthetized rodents have shown that single neurons in NTS respond to taste and can be modulated by more than one taste quality [80, 81]. In addition to chemosensory information, the NTS also receives somatosensory information from the oral region via the cranial and trigeminal nerves. In line with this anatomical organization, single cell recordings have shown that taste responsive neurons in the NTS are also modulated by licking and tactile stimulation of the oral region [82-84]. These findings demonstrate that the gustatory system integrates information from multiple taste qualities and somatosensory features at the early

stages of the ascending pathway. In rodents, gustatory information is then relayed from the NTS to a second brainstem nuclei; the parabrachial nucleus (PBN) in the pons, where neurons show both broadly and narrowly tuned responses to chemosensory stimuli [85, 86] . Similar to the NTS, PBN also receives inputs from other sensory modalities including somatosensory input from the orofacial regions. Single unit recordings in alert rodents show that firing pattern of PBN neurons can be modulated by licking in addition to chemosensory stimulation [85].

The ascending gustatory pathway then diverges from the PBN to two main regions; the gustatory thalamus (ventral posteromedial thalamic nucleus, VPMpc) and the central amygdala (CeA). These two diverging pathways through VPMpc and CeA are thought to process two distinct features of taste stimuli: chemical identity and hedonic value (i.e., palatability and aversiveness) of tastants respectively. However recent evidence suggests that, while each pathway might primarily be devoted to processing a specific feature, the hedonic and identity related information is not entirely segregated in either pathway [69, 87].

Neurons in VPMpc are broadly tuned to tastants [87] and, similar to the upstream regions in the gustatory system, respond to multiple modalities such as the tactile and thermal features of taste stimuli [88, 89]. The VPMpc is the main afferent sensory input to gustatory cortex and in addition to providing gustatory cortex with taste related information, this projection plays an important role in maintaining the state of GC network activity as shown by inactivation of VPMpc leading to slow oscillations in GC [69]. The gustatory cortex, the primary sensory cortical region devoted to taste-related information processing, is crucial for processing complex features of taste stimuli and integrating this information with brain-wide circuits to inform taste related behaviors.

While the canonical gustatory pathway begins with the taste receptor cells and continues with NTS, PBN, VPMpc and GC, there are many other brain regions that have reciprocal connections with the gustatory system and that contribute to diverse aspects of taste processing. It has been shown that the basolateral and central amygdala as well as the mediodorsal thalamus are reciprocally connected with gustatory areas [90-93]. The interconnectivity with these limbic regions is thought to be important for taste related associative learning and subjective value of taste stimuli [94, 95]. Furthermore, gustatory regions are reciprocally connected with orbitofrontal and anterior cingulate cortex, both of which are higher order cortical regions thought to act as associative taste cortices [96, 97]. Last but not least, the lateral hypothalamus, a key region involved in energy homeostasis and in regulating feeding behaviors, is interconnected with gustatory regions [98-100]. This connectivity is thought to be important for modulating taste processing in a hunger and satiety dependent manner. A summary of gustatory pathway connectivity is provided in Figure 3A.

Overall, the findings summarized above demonstrate that the gustatory system is highly interconnected with other sensory modalities throughout the ascending pathway. Single neuron recordings reflect this extensive convergence with broadly tuned, multimodal responses to diverse features of taste stimuli. The sections below will discuss the anatomical and functional properties of gustatory cortex in detail.

1.2.2. Organization of Gustatory Cortex

The gustatory cortex, positioned on the lateral surface of the brain, is part of the insular cortex. As shown in Figure 3B, it is neighbored by the somatosensory and olfactory cortices on its dorsal and ventral borders respectively. In contrast to other primary sensory cortices that are cytoarchitecturally uniform, GC has three distinct laminar patterns corresponding to three subdivisions along its dorsal-ventral axis. Granular GC, located most dorsally, displays a typical six layered organization with a clear layer 4, while dysgranular GC, located more ventrally, has a disappearing layer 4. Finally, agranular GC, located most ventrally, just above the piriform cortex, does not contain an identifiable layer 4. The change of laminar organization along the dorsal-ventral axis suggests that the insular cortex might be a transitional area between the neocortical, somatosensory region and the paleocortical, olfactory region [101].

Tracing studies have revealed that inputs to GC can preferentially target specific subdivisions. Nuclei along the ascending taste pathway preferentially target the dorsal portions of GC (the granular and dysgranular subdivisions), the limbic projections from amygdala (AM), and mediodorsal thalamus (MD) and projections from the lateral hypothalamus (LH) and prefrontal cortices (ACC and OFC) mainly target ventral portions of GC (dysgranular and agranular subdivisions) [90]. While the inputs preferentially (but not exclusively) target specific subdivisions, there is extensive interconnectivity among those subdivisions, suggesting that all the inputs are ultimately integrated and processed across all subdivisions of GC [102, 103].

The ascending gustatory pathway to GC is not merely a feedforward pathway, but it has many feedback projections from downstream areas including the GC to NTS, PBN and VPMpc feedback [90]. The GC activity can modulate VPMpc either directly through corticothalamic projections [90, 104] and/ or indirectly through its projections to reticular nucleus of thalamus [105] which then sends inhibitory projections to VPMpc. Outside of the gustatory pathway, GC projects mainly to regions it receives inputs from, including the LH, AM, MD [90], and ACC [106], but it also sends projections to nucleus accumbens [107] to mediate reward processing and to endopiriform nucleus [108] to mediate integration of olfactory and taste stimuli.

With regards to how different cell types are distributed across lamina and subdivisions, a comprehensive view can be obtained for interneurons from the in situ hybridization data available at the Allen Brain Atlas (*http://mouse.brain-map.org/*). As a clear genetic classification of excitatory neurons is not yet available, I will limit my investigation of this data set to the distribution of genetically identified interneuron subtypes. As summarized in Figure 4, visual inspection of these data reveals that subtypes of interneurons have distinct distribution patterns across the dorsal-ventral axis and across layers. Parvalbumin expressing (PV) interneurons are exclusively found in granular and to a lesser extent in dysgranular regions of GC. The density of PV neurons is greater in L4 and L5 and sparser in superficial layers. Moving more ventrally, PV neurons diminish in parallel with the disappearance of L4 and are visually absent in cortical regions that do not follow the typical 6-layer organization. Somatostatin positive neurons (SOM), unlike the PV neurons are distributed evenly across all three subdivisions of GC and are concentrated in L4 and L5. Lastly, vasoactive intestinal peptide expressing neurons (VIP), also found in all three subdivisions, are strongly biased to the superficial layers of GC. These results suggest that GC does contain all three categories of non-overlapping interneuron populations

with deep layers containing mostly PV and SOM interneurons and superficial layers containing almost exclusively VIP neurons.

Overall, the findings summarized in this section demonstrate that GC is organized in different, but intercommunicating, subdivisions. While the functional specialization of these subdivisions is still a matter of debate, experimental evidence suggests a high degree of integration of sensory and limbic information.

A. B.

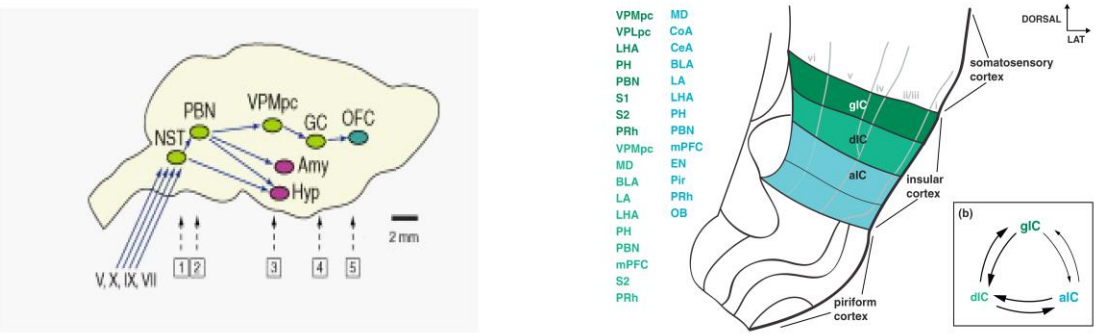

Figure 3. Ascending Gustatory Pathway and Gustatory Cortex Connectivity

A. Schematic of ascending gustatory pathway. Taste information arriving from the periphery is carried to brain stem nuclei NTS via the cranial nerves (V, X, IX, VII). NTS projects to a second brain stem nucleus, the PBN, which then sends taste related information to gustatory thalamus (VPMpc). This thalamic nucleus sends its projections to primary gustatory cortex (GC). Outside of the main gustatory regions, amygdala (Amy), hypothalamus (Hyp) and orbitofrontal cortex (OFC) receive taste information from the regions along the ascending gustatory pathway. Adapted from [79].

B. Schematic of gustatory cortex organization and long range inputs. Coronal view of GC shows the three cytoarchitecturally distinct regions along the dorsal-ventral axis. The laminar organization is outlined in light grey. The most dorsal, dark green region corresponds to granular GC, light green corresponds to dysgranular GC and blue region corresponds to agranular GC. The long range inputs onto GC are color coded according to which portion of the GC they preferentially target. The inset displays the reciprocal interconnectivity among the three subdivisions of GC. *Abbreviations;* aIC: agranular insular cortex, BLA: basolateral amygdala, CeA: central amygdala, CoA: anterior cortical nucleus, dIC: dysgranular insular cortex, EN: endopiriform nucleus, gIC: granular insular cortex, LA: lateral amygdala, LHA: lateral hypothalamic area, MD: mediodorsal thalamic nucleus, mPFC: medial prefrontal cortex, OB: olfactory bulb, PBN: parabrachial nucleus, PH: posteriorhypothalamic nucleus, Pir: piriform cortex, PRh: perirhinal cortex, S1: somatosensory cortex, area 1, S2: somatosensory cortex area 2, VPLpc:ventroposterolateral thalamic nucleus, parvicellular part, VPMpc: ventroposteromedial thalamic nucleus, parvicellular part. Adapted from [101].

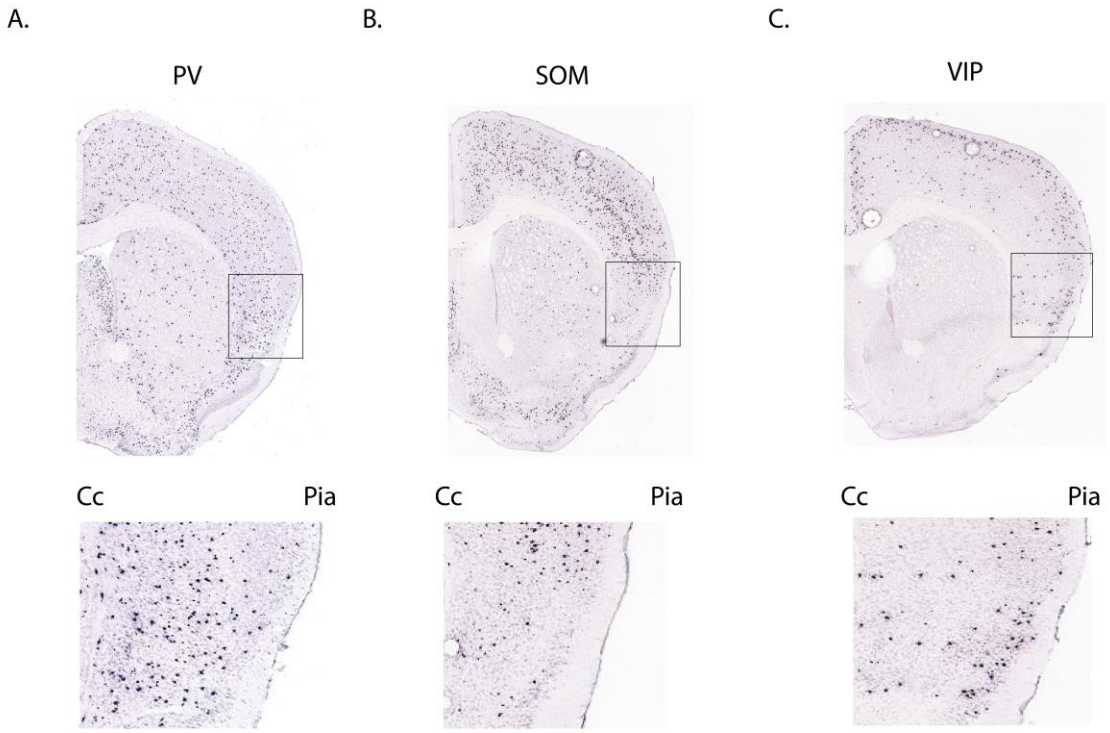

Figure 4. Distribution of Inhibitory Neuron Subtypes in GC

Coronal sections (1 mm anterior of Bregma) showing in situ hybridization data for three different markers of inhibitory interneurons. Black squares outline the gustatory cortex. Bottom panels show zoomed in view of the gustatory cortex. Abbreviations; Cc: corpus collosum, PV: parvalbumin, SOM; somatostatin, VIP; vasoactive intestinal peptide. Data obtained from Allen Brain Atlas database.

A. PV expressing interneurons are dispersed throughout L2-L6 of all three subdivisions of GC.
B. SOM expressing interneurons are concentrated in L2/3 and L4 in granular GC. The density of SOM neurons greatly decrease in dysgranular and agranular GC.
C. VIP expressing interneurons are concentrated in L2/3 of GC.

1.2.3. Lamina and Cell Type Specificity of Thalamic and Amygdalar Axonal Projections to Gustatory Cortex

Apart from the preferential targeting of inputs across the subdivisions, anterograde tracing studies revealed that gustatory thalamus and basolateral amygdala display distinct projection patterns across GC lamina ([90], Stone et., al., *unpublished*). In adult rats, the VPMpc projections target all layers with a slight bias towards L3 and L4 showing a more diffused pattern compared to the thalamocortical projections in other sensory systems where layer 4 receives the densest projection. Amygdalar projections on the other hand predominantly target superficial and deep layers, with sparse axons in the middle layers. Dual anterograde tracer injections clearly demonstrate that amygdalar and thalamocortical axonal projections have distinct laminar distribution across GC.

In the first study to investigate the synaptic properties of amygdala input onto GC, Haley et. al., demonstrated using optogenetic and slice electrophysiology techniques that BLA projects to both excitatory and inhibitory neurons within GC [92]. Furthermore, the strength of these BLA synaptic inputs changes in a layer and cell-type specific fashion. Excitatory neurons in superficial layers receive stronger inputs compared to excitatory neurons in deep layers. Interestingly the opposite pattern is observed for SOM neurons where deep layers received stronger input compared to the superficial neurons. Lastly, inputs onto the PV neurons do not show laminar differences. This is the first study to demonstrate that the strength of a given projection onto GC varies in a layer and cell type dependent fashion.

Taken together, these results suggest that there might be differences in functional properties of gustatory cortex neurons based on the distinct connectivity and relative input strength among layers and cell types.

1.3. Functional Properties of Neurons in Gustatory Cortex

Studies investigating the functional properties of GC neurons have primarily relied on extracellular recordings of spiking activity in anesthetized and alert rodents. While there has been an increase in the number of imaging studies using voltage sensitive dyes [102, 103, 109, 110] and calcium indicators [111] in the past decade, most of our understanding of single neuron GC neural activity comes from electrophysiological studies. This section will focus on these studies and will review response profiles and functional properties of gustatory cortex neurons.

1.3.1. Taste Coding in GC

Early studies in anesthetized rodents have shown that all three subdivisions of GC respond to taste stimuli [112-114]. Taste responses observed in agranular GC, which does not receive direct VPMpc input, are thought to result from the high interconnectivity among the three subdivisions. In anesthetized preparations, the overall taste responsiveness is low [115], and this has been attributed to altered thalamocortical activity due to anesthesia.

As the field moved to studying gustatory function in awake rodents, two main taste delivery approaches were adopted: taste delivery via intra-oral cannulas (IOCs) and taste delivery via a licking spout. The IOC approach was preferred to precisely control the timing and amount of tastant delivered directly into the mouth. Studies across many laboratories, where tastants were delivered directly into the oral cavity in awake rodents, have found that single neurons in GC respond to multiple tastants and differentiate across tastants with time-varied firing rate patterns [18, 97, 116]. Figure 5A illustrates one representative single neuron response to IOC taste delivery. Similar to the NTS, PBN and VPMpc, GC neurons also show broadly tuned responses. Furthermore, experiments using IOCs revealed a particular structure in the modulation of firing rates evoked by taste. The first 250 ms of stimulus evoked activity encode somatosensory information related to the fluid touching the mouth. Taste information emerges in the 250/500-1000 ms interval and is followed by a third epoch (1000-2500 ms) where the hedonic component of each taste stimulus is encoded [116].

Experiments in which animals licked a spout to obtain taste solutions unveiled stimulus-evoked response patterns that differed from those observed in IOC experiments. These studies have reported that majority of GC neurons' firing patterns is structured by licking rhythmicity [20, 117, 118] as shown in Figure 5B. Another important difference between the two experimental conditions is the onset of taste coding. Unlike the IOC experiments, in licking animals, single neurons show taste specific responses as early as 70-120 ms after contact with the taste solution [117]. Although firing patterns in spout vs IOC deliveries were very different, studies using both methods reported broadly tuned taste responses. The different response dynamics evoked by the two distinct sampling paradigms highlight how the behavioral state of the animal plays a key role in shaping cortical responses and sensory processing in GC.

In addition to studying the temporal dynamics of taste responses, research in the field has also focused on the spatial representation of stimulus-evoked activity in GC. Results from imaging studies have suggested that different taste qualities are represented in different regions of GC. Using *in vivo* intrinsic imaging in anesthetized rats, Accolla et. al., [110] have shown that the four primary taste qualities are represented by distinct spatial patterns across GC. While different tastants preferentially activated distinct parts of GC, their spatial representations were overlapping and no single region was exclusively representing a single taste quality. A more recent study using two-photon calcium imaging in anesthetized mice has found completely segregated taste representations in GC, where a given taste responsive region only responds to a single taste quality [111]. These results stand at odds with the findings from electrophysiology studies where single neurons respond to multiple taste stimuli and nearby neurons display distinct stimulus selectivity [119]. One explanation for the observed differences in electrophysiological versus imaging studies may relate to the reliance on distinct preparations. Indeed, imaging experiments have been performed in anesthetized rodents. It is possible that anesthesia alters the excitation/inhibition balance in cortex, changing the mode of sensory processing. Alternatively, these findings could arise from differences in the lamina recorded, with imaging studies mainly reflecting responses of superficial layer neurons. However, very little is known about whether taste responses in GC are layer dependent.

While no study to date has compared the functional properties of GC neurons belonging to distinct layers and cell types in awake animals, a recent study has investigated taste responses of pyramidal and inhibitory neurons in anesthetized rats. This study has shown that inhibitory neurons had shorter response latencies and longer response durations compared to the pyramidal neurons. Furthermore, the authors have reported that the inhibitory neurons had narrow taste tuning while pyramidal neurons showed broadly tuned taste responses [120].

Overall, the results presented in this section illustrate that GC neurons can show broadly tuned taste responses under different taste delivery conditions albeit with varied response patterns. However, the degree to which neurons in distinct cell categories and layers display distinct response patterns and tuning properties is still unexplored.

1.3.2. Beyond Taste Coding

Reflecting the rich interconnectivity with regions processing sensory information pertaining to other modalities, neurons in gustatory cortex respond to somatosensory, olfactory, visual, and auditory stimuli [21]. While GC can respond to all cross-modal stimuli, the representation of olfaction and touch is greater compared to other modalities. This finding is consistent with the ecological relevance of these modalities in taste. Additional experiments showed that pairing of cross-modal stimuli with taste delivery increases the percentage of neurons responding to cross-modal stimuli, suggesting that cross-modal representations can be shaped by learning [21]. Indeed, neurons in GC can effectively encode cues anticipating the availability of taste. Classical and instrumental conditioning experiments demonstrate that GC neurons can respond to auditory cues predicting the general or the specific expectation of taste [21-23]. Figure 5C and 5D show representative examples of GC neurons responding to cross-modal stimuli and auditory cues predicting tastes respectively.

The representation of somatosensory stimuli in GC has been widely observed in studies with licking animals, where taste consumption inherently has a somatosensory component. In these studies, authors have reported that the firing activity of GC neurons is strongly patterned by licking rhythmicity (6-12 Hz), even when licks do not result in fluid delivery [20, 117, 118]. These results are consistent with the anatomical and physiological findings showing that somatosensory information from the oral region converges onto gustatory nuclei along the ascending gustatory pathway (NTS, PBN and VMPpc).

In addition to encoding the somatosensory and olfactory features that accompany most taste stimuli, GC also carries information pertaining to the hedonic value of tastants. Evidence for this comes from conditioned taste aversion (CTA) studies, where animals develop an aversion to sucrose solutions after sucrose is paired with gastric malaise. These studies have shown that GC responses to sucrose are altered after the CTA [24, 25].

All in all, the functional properties summarized above reflect the rich connectivity of GC with other sensory, limbic and cognitive brain regions and show that GC not only processes taste related information, but also cross-modal, anticipatory and affective signals. How these functional responses emerge in gustatory circuits and whether neurons belonging to different layers and cell types display distinct functional properties is unknown. The dissertation work presented here aims at addressing this gap in the literature.

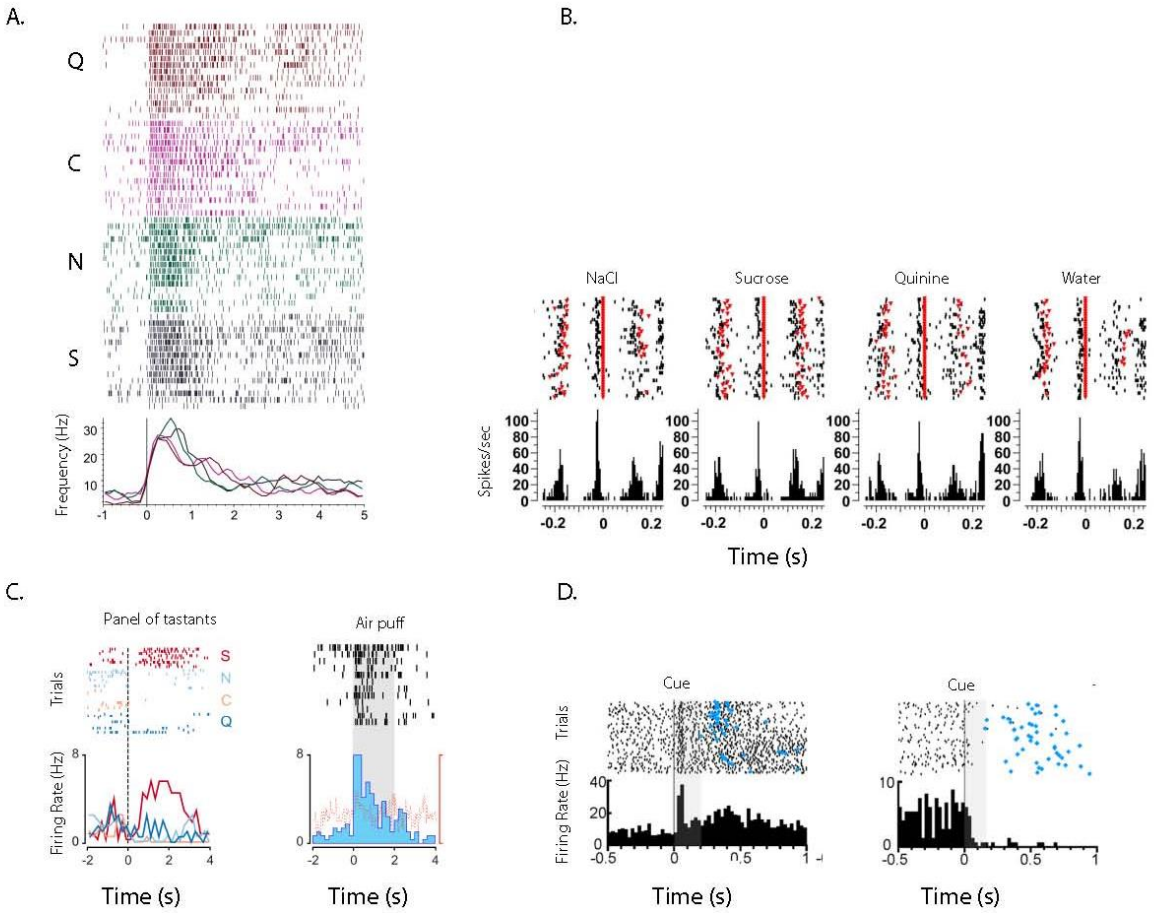

Figure 5. Functional Properties of GC Neurons

- **A.** Response dynamics of a single GC neuron to four intraorally delivered taste stimuli. Time 0 indicates the onset of the taste delivery. Top panels display raster plots where each tick mark represents an action potential. Responses to each of the four stimuli are grouped and color coded for easy visualization. Bottom panel displays PSTHs for all taste responses. This neuron display broadly tuned responses to all four stimuli with long lasting firing rate modulations. Panel adapted from [97].
- **B.** Response dynamics of a single GC neuron to four taste stimuli in licking animals. Time 0 indicates the animals contact with a taste solution. Each black tick is an action potential and each red dot is a lick. Each panel represents the raster (top) and PSTH (bottom) of the neuron's response to one of the four stimuli presented. The activity of this neuron shows a clear relationship to the licking cycle. Panel adapted from [117].
- **C.** Response dynamics of a single GC neuron to a panel of four tastants and air puff to the whiskers. Left panel, time zero indicates onset of the intraoral taste delivery. Top panel shows the raster plot color coded for each tastants. Bottom panel shows the PSTH for four tastes. This neuron differentially responds to sucrose and quinine with different intensity and temporal dynamics. Right panel, show the response of the same neuron to the air puff stimulation of the whiskers. Time 0 indicates onset of the air puff. The raster and PSTH illustrate that this GC neuron respond to cross-modal stimuli in addition to taste (as shown on the left panel). Panel adapted from [21].

D. Response dynamics of single GC neurons to auditory cue that predicts a taste delivery. Time 0 indicates auditory cue onset. Top panels show rasters and bottom panel shows PSTHs. Blue dots mark the onset of intraoral taste delivery in each trial. Left panel, representative neuron that displays an excitatory response to the cue onset. Right panel, representative neuron that displays an inhibitory response to the cue onset.

1.4. Experimental Design and Dissertation Structure

For the work presented in this dissertation, we designed and conducted experiments to investigate functional differences of gustatory cortex neurons belonging to different lamina and cell types in awake mice. The main topics addressed in this dissertation are as follows 1) laminar and cell type differences in baseline and anticipatory activity in gustatory cortex 2) laminar and cell type differences in stimulus evoked activity 3) laminar and cell type differences in taste coding 4) convergence of distinct functional phenomena in gustatory cortex neurons.

The findings presented in this dissertation are based on extracellular, single unit recordings targeting deep and superficial layers of gustatory cortex in alert, head-restrained mice performing a licking paradigm to different tastants. In this experimental paradigm, mice were trained to sit comfortably in head-restraint and to lick in a stereotyped fashion a spout containing one drop of taste solution, chosen randomly from a panel of five stimuli. This experimental protocol was selected to ensure stereotyped licking behavior across different tastants. To target deep and superficial layers of gustatory cortex, two complementary approaches were taken. In the first experimental preparation, we used dorsally implanted chronic electrodes that provided high yield. In a second preparation, we performed acute recordings from the lateral surface of gustatory cortex which provided high precision in targeting laminae. The results of these experiments are presented in the following chapters.

In Chapter 2, I present results on differences in activity for neurons belonging to different layers and types (putative excitatory and inhibitory) for the following epochs: baseline, cue, pre-licking, licking and taste processing. I present results on firing rate changes that occur prior to animal's contact with taste solution. The temporal dynamics of this pre-stimulus modulation are discussed particularly in context of its possible behavioral contingencies. I discuss two important findings regarding the response dynamics of gustatory cortical neurons in stimulus-evoked epoch. First, by warping the neural data according to the rhythmic lick cycles, I show that neurons in gustatory cortex show spiking patterns that are phase locked to the lick cycle. By quantifying this phase locking, I show that this phenomenon occurs more strongly in pyramidal neurons of gustatory cortex. In the next part of the chapter, I show our findings regarding taste coding in gustatory cortex focusing on temporal dynamics of taste coding in licking animals and how breadth of tuning varies of cell type categories. Finally, I discuss to what extent these various phenomena that we observe in gustatory cortex converge on the same neurons. The results reveal that neurons with anticipatory, sensorimotor and taste coding features show significant overlap, indicating that these features, potentially representing independent inputs can converge on the same neurons within gustatory cortex.

In Chapter 3, I discuss the implications and significance of findings presented in this work and how they relate to the findings from previous work in the literature. Lastly, in Chapter 4, I detail the experimental and analytical methods adopted for this study.

Chapter 2

Results

Single unit activity was recorded from 24 head restrained mice performing a licking paradigm. This paradigm was designed to standardize licking to different taste stimuli. As shown in Figure 6A, each trial began with an auditory cue and was followed by the protraction of the lick spout containing a single drop of solution chosen randomly from a set of five stimuli (sucrose, salt, citric acid, quinine and water). Mice had to lick at a minimum of 7 Hz frequency for at least six consecutive licks for the trial to be considered correct. On the sixth lick, mice received a single drop of water to rinse the mouth. The spout retracted 1 second after the sixth lick. Consecutive trials were separated by a 3 second inter-trial interval. After training, mice displayed stereotyped licking behavior across different stimuli throughout the recording session (Fig. 6B) (inter-lick interval mean = 0.135s ± 0. 035s). On average mice performed 100 ± 34 trials in a session (session duration: 27 ± 8.2 min.). Trials in which animals did not initiate licking, execute enough licks or maintain the required lick frequency were considered error trials and followed by a 20 second time-out period. Error trials constituted a negligible portion of the total trials in the recording sessions (0.05%) and were excluded from further analysis.

2.1. Layer and Cell Type Identification

To record firing activity of gustatory cortex (GC) neurons we relied on chronic and acute extracellular recordings (Fig. 7F) from deep (Fig. 7E) and superficial (Fig. 7D) layers of GC in alert mice. Deep and superficial layers were defined based on the position of recording site relative to Layer 4 (see *Methods, Layer assignments*). Recordings were targeted to the portion of GC that receives direct input from the gustatory thalamus (VPMpc) as shown by retrograde tracer injections (Fig. 7A-C). This portion of GC (stereotaxic coordinates from bregma: AP: +1.1 mm, ML: 3.5 mm, DV: -2.5 mm to -2.7 mm), which correspond to granular/dysgranular GC, can be targeted from the lateral surface during acute recordings as it corresponds to the intersection between the medial cerebral artery and the rhinal veins [111].

A total of 223 single units were isolated across animals and sessions, with 147 units recorded from deep layers and 76 units recorded from superficial layers. Neurons were further classified into putative excitatory and inhibitory cell type categories based on the width of extracellularly recorded action potential waveforms (Fig. 6C). The width of action potentials showed bimodal distribution (middle panel, Fig 6C). Using k-means clustering, 23% of units (51/223) with narrow waveforms (mean = 203.4μs, std = 49.5μs) were classified as putative inhibitory neurons and 77% of neurons (172/223) with wide waveforms (mean = 375.9μs, std =

101.1μs) were classified as putative excitatory neurons. The population of putative inhibitory neurons showed significantly higher baseline firing rates compared to putative excitatory neurons, further confirming the classification ($p < 0.0001$, Kolmogorov-Smirnov goodness of fit test, Fig. 6C, right panel).

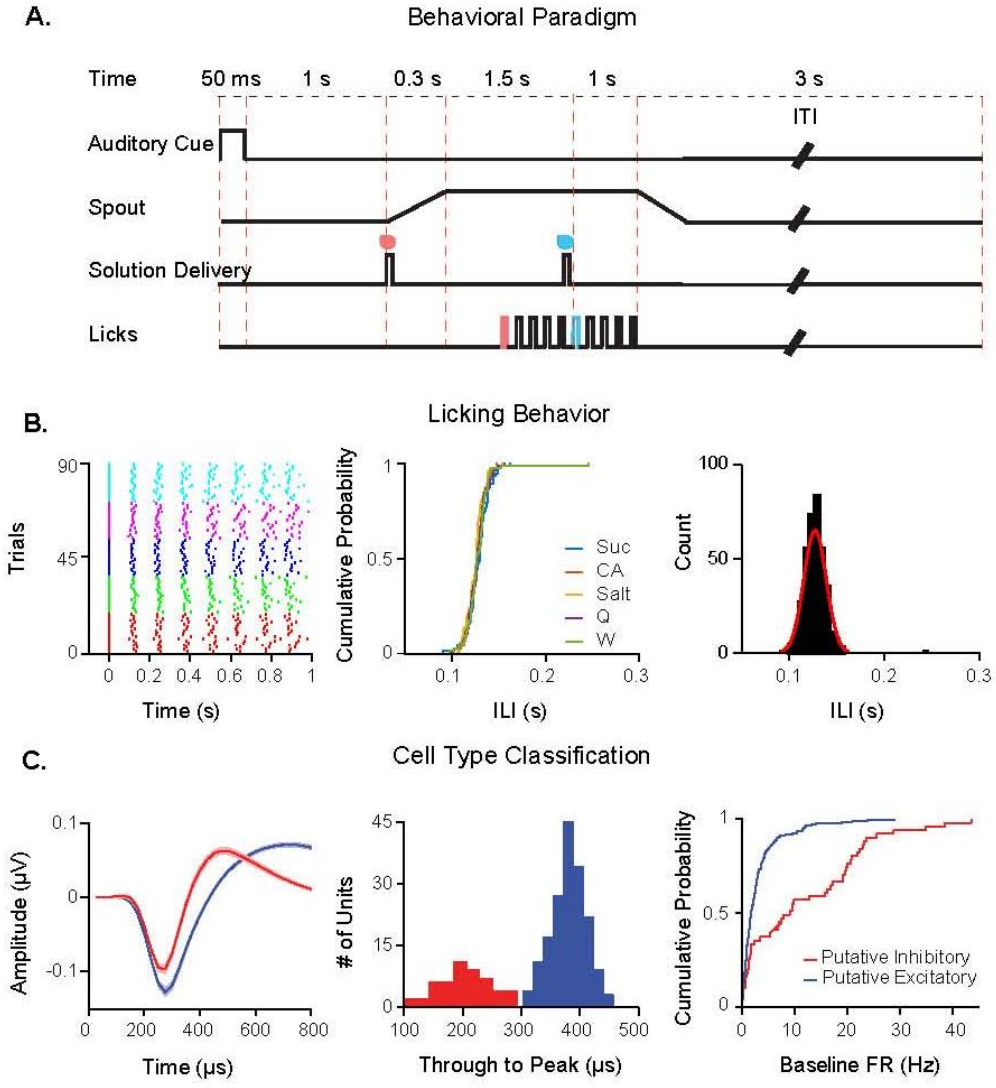

Figure 6. Behavioral Paradigm and Methods

A. Schematic representation of the behavioral paradigm. Each trial began with an auditory cue (50ms) and was followed, after 1s, by the protraction of a lick spout containing a single drop

of solution. In each trial, the drop of solution (~ 2µL), was chosen pseudorandomly, from one of five stimuli: water, sucrose, salt, citric acid and quinine. In the subsequent four licks mice did not receive additional solution and received a drop of water (~ 2 µL) after the fifth lick to rinse the mouth.

B. Representative licking behavior from a single session. Left panel shows licking behavior for all five stimuli across the session. Trials are reordered and grouped by stimulus type for visualization (color-stimulus association same as in panel A). Each row is a trial and each dot represents a lick, all trials are aligned to the first lick. Only the first seven licks of each trial are shown. Middle panel shows the cumulative distribution function of the interlick interval (ILI) for each type of taste trial. Right panel shows the distribution of ILI's for all trials in the session.

C. Classifying cell types based on action potential waveform. Left panel shows average waveforms for putative inhibitory neurons (in red) and putative pyramidal cells (in blue). Middle, distribution of action potential widths for putative inhibitory (in red) and putative pyramidal (in blue) neurons. Right, cumulative distribution function of baseline firing rates of putative inhibitory and putative pyramidal neurons.

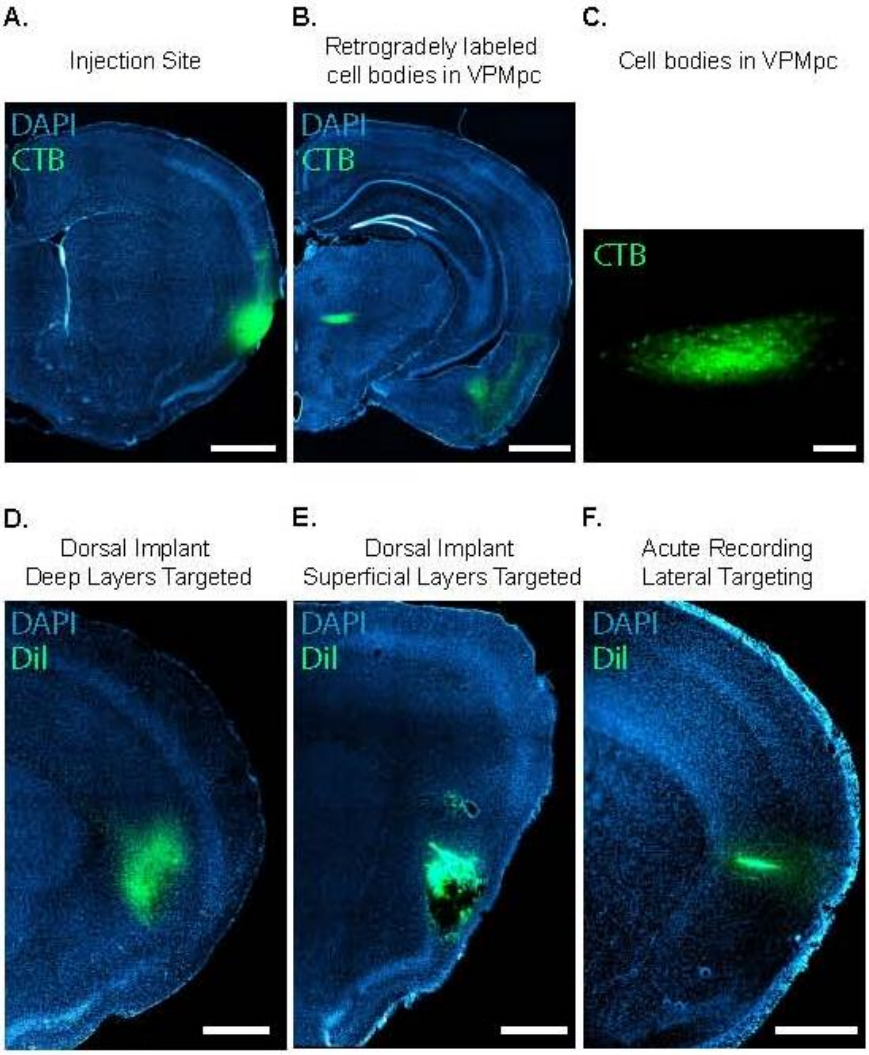

Figure 7. Retrograde Tracer Injections and Recording Site Confirmation

- **A.** Retrograde tracer injection into GC. Coronal section showing retrograde tracer CTB 555, injection site (Bregma: + 0.8mm). Nuclear counterstain with DAPI, pseudocolored in cyan. CTB 555 is shown in green. Scale bar is 1mm.
- **B.** Retrogradely labeled cell bodies in VPMpc. Coronal section (Bregma: -2.4mm) shows retrogradely filled cell bodies in VPMpc, as well posterior BLA and piriform cortex. Scale bar is 1mm.
- **C.** 20X magnification of retrogradely filled cell bodies in VPMpc in same coronal section as B. Nuclear counterstain with DAPI. CTB 555 is shown in green. Scale bar is 0.1mm.
- **D.** Histology from chronic, dorsal electrode implant targeting deep layers of GC (Bregma: +0.9 mm). Nuclear counterstain with DAPI (pseudocolored in cyan). Tip of the electrode coated in DiI (shown in green). Scale bar is 0.5mm.
- **E.** Histology from chronic, dorsal electrode implant targeting superficial layers of GC (Bregma: +1.0 mm). Nuclear counterstain with DAPI (pseudocolored in cyan). Tip of electrode coated in DiI (shown in green). Scale bar is 0.5mm.

F. Histology from acute recording configuration, electrodes inserted from the lateral side of the brain, entering orthogonal to layers of cortex (Bregma: +1.0mm). Nuclear counterstain with DAPI (pseudocolored in cyan) Electrode coated with Dil (shown in green). Scale bar is 0.5mm.

2.2. Baseline and Evoked Firing Rates of GC neurons are layer and cell type specific

Upon classifying neurons based on laminar position and action potential waveform, we created four categories: deep layer pyramidal neurons, DP, (101/223), deep layer inhibitory neurons, DI, (46/223), superficial layer pyramidal neurons, SP, (71/223) and superficial layer inhibitory neurons, SI, (5/223). Box plots of baseline and stimulus-evoked firing rates of all four categories of neurons are shown in Figure 8A. Table 1 summarizes the descriptive statistics for firing rates of each category.

Baseline firing rates were significantly different across categories ($p < 0.00001$, Kruskal-Wallis test) with DI neurons showing greater baseline firing rates compared to DP, SP and SI neurons (for all, $p < 0.001$, post-hoc multiple comparisons with Bonferroni correction). The baseline firing rates did not differ among DP, SP and SI neurons. Stimulus evoked firing rates were also significantly different across categories of neurons ($p < 0.00001$, Kruskal-Wallis), with DI neurons showing significantly greater firing rates compared to DP and SP neurons (both $p < 0.0001$, post-hoc multiple comparisons with Bonferroni correction). Interestingly, while DP and SP showed similar firing rate distributions at baseline, DP neurons had significantly higher firing rates in the stimulus evoked period compared to SP neurons ($p = 0.01$, post-hoc multiple comparisons with Bonferroni correction).

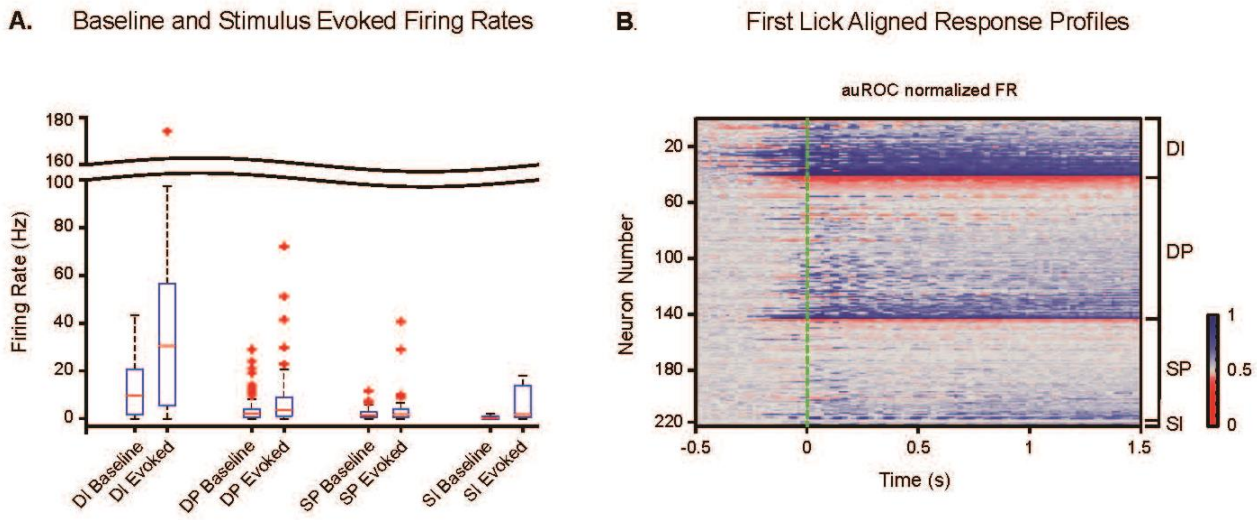

Figure 8. First-lick Aligned Response Patterns of Gustatory Cortex Neurons

A. Box plots for baseline and stimulus evoked firing rates in each category of neurons. Median value of each category is plotted as red horizontal line, lower and upper boundaries of the box plot represent 25th and 75th percentile respectively. Outliers are plotted as red crosses.

B. Heat map of auROC normalized population activity aligned to the first lick. Time 0 indicates the first lick. Neurons are grouped into categories according to their layer and putative cell type. Each category is sorted in ascending order by their average firing rate in the stimulus evoked (0 - 1.5s) interval. In the pseudo-colored activity plot, excitatory responses (auROC value > 0.5) in a given bin (20ms bin) are shown in blue and inhibitory responses (auROC value < 0.5) are shown in red.

Table 1. Summary Statistics for Baseline and Evoked Firing Rates of GC Neurons

Descriptive statistics	**Mean ± SEM**	**STD**	**Median**
DI-Baseline	12.98 ± 1.64	11.12	9.61
DI-Evoked	35.59 ± 5.12	34.73	30.55
DP-Baseline	3.80 ± 0.51	5.16	2.06
DP-Evoked	7.07 ± 1.04	10.48	3.63
SP-Baseline	2.0 ± 0.23	1.98	1.51
SP-Evoked	3.23 ± 0.70	5.89	1.87
SI-Baseline	0.62 ± 0.43	0.95	0.12
SI-Evoked	6.66 ± 3.63	8.12	1.81

2.3. GC Neurons Display Pre-Stimulus Modulations

We first investigated whether single GC neurons display modulations to the auditory tone (cue) at the onset of trials by aligning all trials to the tone onset and classifying neurons as cue responsive when firing rates in the 500 ms interval following the cue displayed significant changes from baseline firing rates. This analysis revealed that 10% of GC neurons showed modulations following the cue, and there were no significant differences in prevalence of cue responses across cell categories (*data not shown*).

Next, to visualize the time course of firing rate modulations for the entire population, each neuron's session average firing activity was normalized using auROC normalization (see *Methods*) and plotted in a single row as a heat map (Fig. 8B). In the heat map, excitatory deviations from baseline firing rates are shown in blue and inhibitory deviations from baseline firing rate are shown in red. Population activity aligned to the first lick illustrates that in a subset of neurons the firing rate modulations begin before animal's tongue contacts the solution.

To investigate the pre-stimulus activity observed in Fig. 8B, we classified each neuron either as pre-stimulus modulated or non-pre-stimulus modulated based on the presence or absence of significant changes from baseline firing rates in the 500 ms interval prior to the first-lick. Overall, 60% of neurons (135/223) in GC showed pre-stimulus modulations with 38% (85/223) showing excitatory and 22% (50/223) showing inhibitory pre-stimulus modulations. Rasters and PSTHs of two representative neurons that display excitatory (left) and inhibitory (right) firing rate changes prior to the first-lick, are plotted in Figure 9A. The relative proportions of pre-stimulus modulated neurons are significantly different across four categories of neurons (DP: 60%, 61/101, DI: 89%, 41/46, SP: 41%, 29/71, SI: 80%, 4/5), ($p < 0.0001$, Chi-Squared test) (Fig. 9B). A greater proportion of deep layer neurons (69%, 102/147) display pre-stimulus modulations compared to superficial layer neurons (43%, 33/76) ($p < 0.001$, Chi-Squared test), and a greater proportion of inhibitory neurons (88%, 45/51) display pre-stimulus modulations compared to pyramidal neurons (52%, 90/172) ($p < 0.0001$, Chi-Squared test). These results show that while neurons in all categories display pre-stimulus modulations, pre-stimulus modulation is strongly biased to deep layer inhibitory neurons.

Next, we investigated whether the proportion of neurons excited or inhibited in the pre-stimulus period differed across layers and cell types (Figure 9C). DP and SP display a similar percentage of neurons that are either excited or inhibited in the pre-lick period (DP excitatory 54 %, 33/61, inhibitory: 46%, 28/61; SP, excitatory: 45%, 13/29, inhibitory: 55%, 16/29). On the contrary, larger proportion of DI neurons shows excitatory modulations during the pre-stimulus phase compared to inhibitory modulations (excitatory modulations: 85%, 35/41 vs inhibitory modulations: 15%, 6/41). The few SI neurons recorded are exclusively excited in the pre-lick phase. Figure 9C features the population-PSTHs for the different groups of pre-stimulus modulated neuron (DP, DI, SP and SI, either excited or inhibited). Visual inspection of

population-PSTHs, confirmed by quantification, reveals an interesting feature of DI neurons. DI neurons that show pre-stimulus excitation feature higher baseline firing activity compared to neurons whose firing is suppressed in the pre-stimulus period. This observation suggests a potential heterogeneity in the group of DI neurons. No such a difference was observed for DP and SP. The observation that DI neurons with distinct baseline firing rates receive distinct pre-stimulus modulations points to the possibility that DI neurons are composed of two functionally distinct categories of neurons. The degree to which these functionally distinct DI neurons constitute molecularly or genetically distinguishable subtypes of inhibitory neurons remains to be investigated.

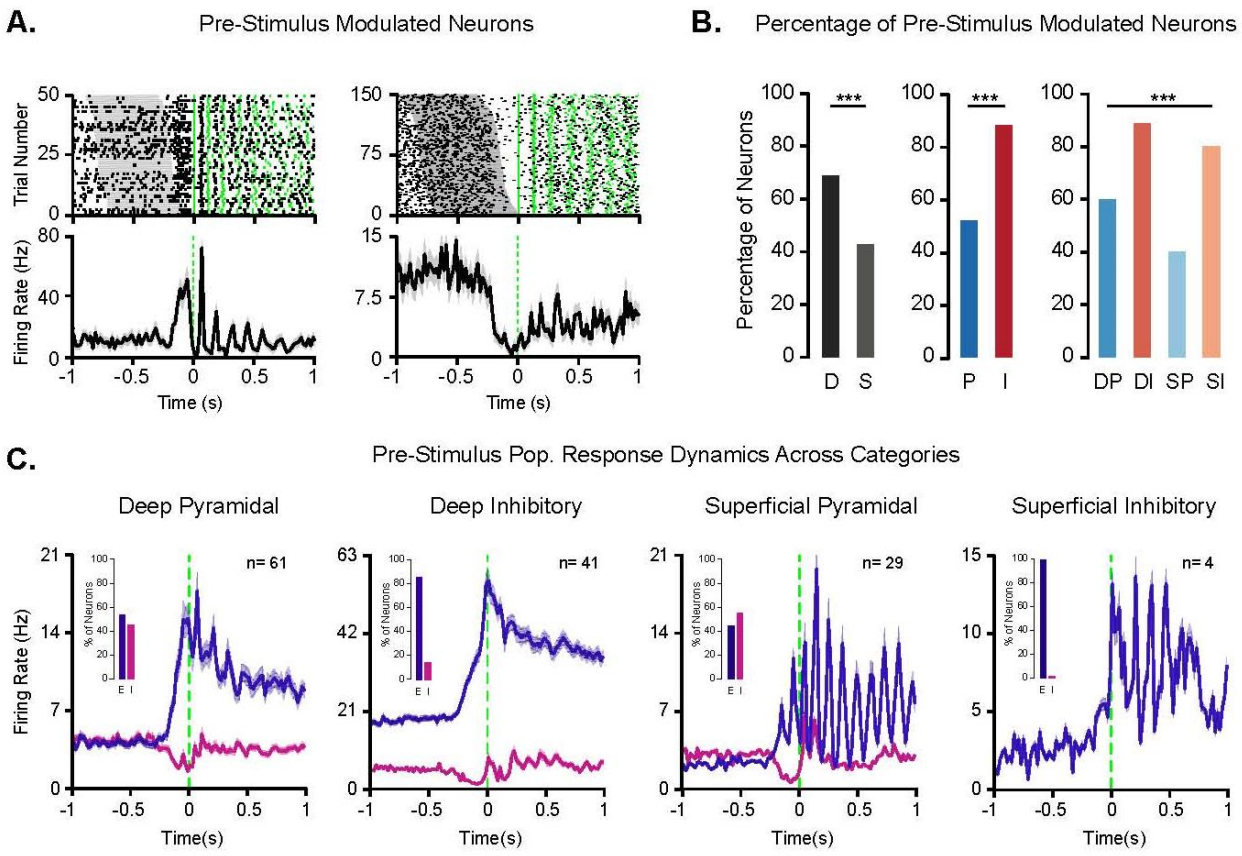

Figure 9. Pre-Stimulus Responses in Gustatory Cortex

A. Representative pre-stimulus modulated single neurons. Left and right panels show rasters (top) and PSTHs (bottom) for a pre-stimulus excited and pre-stimulus inhibited neuron respectively. The trials are aligned to the first lick (time 0) and sorted in ascending order based on spout-offset to first lick time. Gray shaded bars in the raster indicate the duration of spout movement in each trial. Blue dots mark the licks.

B. Percentage of pre-stimulus modulated neurons in each category of neurons. Left panel shows percentage of pre-stimulus modulated neurons in deep (D) and superficial (S) layers. Middle panel shows percentage of pre-stimulus modulated neurons in putative pyramidal (P) and putative inhibitory (I) categories. Right panel shows the percentage of pre-stimulus modulated neurons in deep layer pyramidal (DP), deep layer inhibitory (DI), superficial layer pyramidal (SP) and superficial layer inhibitory neurons (SI). Significance of relative percentages tested using Chi-square test.

C. Pre-stimulus response dynamics across categories. For each category of neurons, population PSTH of pre-stimulus excited (in purple) and pre-stimulus inhibited neurons (in magenta) are shown. The inset shows the percentage of excited and inhibited neurons within the pre-stimulus modulated category. Significance of relative percentages tested using Chi-square test.

2.4. Pre-stimulus Modulations are Aligned to First-lick

First we used change point analysis to detect the onset of pre-stimulus modulations. This analysis revealed that pre-stimulus modulations begin, on average, -0.20 ± 0.01 seconds prior to the first-lick. Next we investigated the behavioral trigger of pre-stimulus activity. As the spout movement occurs very close to the first lick onset, we addressed the possibility that pre-stimulus modulations may be associated with the movement of the spout rather than first-lick onset. We analyzed the spike density of pre-stimulus modulated neurons by aligning it either to the first-lick or to the spout movement onset. The interval between the spout-onset and the first-lick was variable across trials, as mice could initiate licking at any time within the 1 second following the spout onset. We exploited this variability to assess whether pre-stimulus modulations were better aligned to the spout movement or to the first-lick onset. Figure 10 shows raster plots of one representative, pre-stimulus excited neuron aligned to the first-lick (Fig. 10A) and to the spout-movement onset (Fig. 10B). To facilitate visualizing the spike density patterns under the two different alignment configurations, we replotted the raster plots (in the middle panels of Figure 10A and 10B) after excluding the spikes that occur outside of the interval of interest (spout-onset to first lick). Visual inspection of these raster plots reveals that pre-stimulus excitation is aligned to the onset of the first-lick and the response spreads when the activity is instead aligned to the spout movement onset. PSTHs corresponding to these raster plots (plotted in the bottom panel of Figure 10A and 10B) show that, while the total spike count is the same for both alignments, the peak firing rate is higher in the first-lick aligned PSTH compared to the spout-onset aligned PSTH. We extended this analysis to all pre-stimulus excited neurons (n=85), comparing the maximum firing rate in lick aligned versus spout-onset aligned PSTHs. The scatter plot in Figure 10C shows that, for all pre-stimulus excited neurons, lick-aligned PSTHs yield higher peak values compared to spout-aligned PSTHs. Using a second method of analysis, we confirmed this result by comparing the distributions of spike times in spout-offset aligned and first-lick aligned conditions. In this analysis, we only included spikes that occur in the spout-offset to first-lick interval. Given that total spike count is the same across the two alignment conditions, differences in the two distributions is reflective of differences in the spike times relative to the two events. Pooling across all pre-stimulus excited neurons, we observed (as shown in Figure 10C, right panel) that the spike time distribution is skewed toward smaller intervals in first-lick aligned condition, indicating that spikes in the pre-stimulus period occur temporally closer to the first-lick compared to the spout offset. Altogether, these results suggest that pre-stimulus activity is aligned to the first lick rather than spout movement.

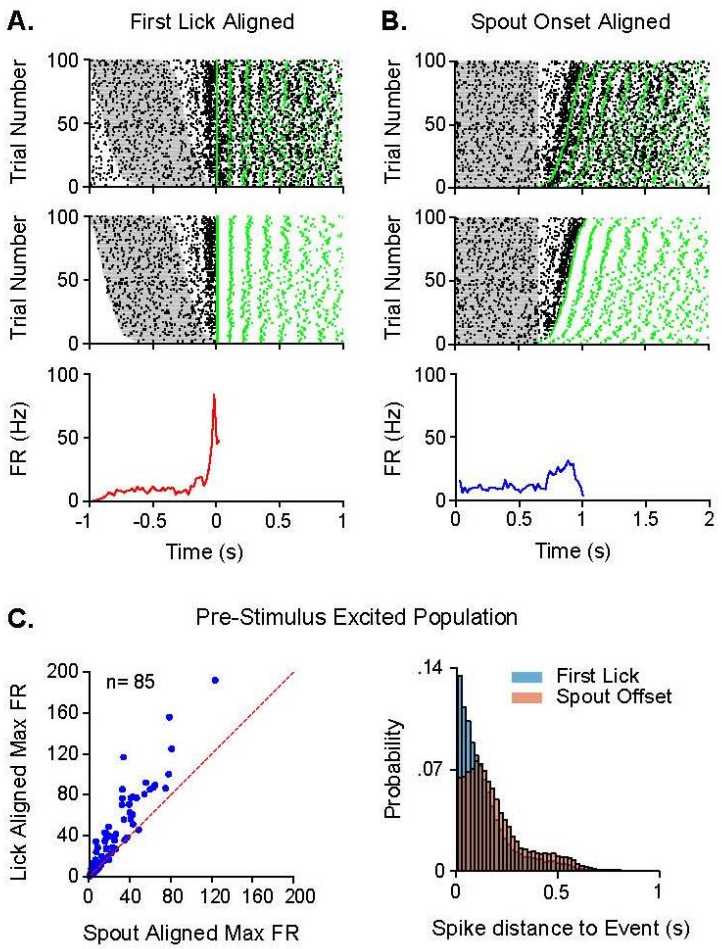

Figure 10. Pre-Stimulus Modulation is Aligned to First Lick

A. Top panel, raster plot of a representative pre-stimulus excited neuron. Trials are aligned to the first lick at time 0. Gray shaded bars represent the duration of the spout movement for each trial. Green dots represent licks. Trials are sorted in ascending order according to the distance from spout-offset to first lick. Middle panel, shows the raster plot of the same neuron as top panel. Only spikes that occur within the spout-onset to first-lick interval are plotted for visualizing alignment of spike times. Bottom panel shows the PSTH corresponding to the middle panel.

B. Raster plot of same neuron as in A, with spikes aligned to the spout onset at time 0. Gray shaded bars represent duration of spout movement. Green dots represent licks. Middle panel only includes spikes that occur within the spout onset to first-lick interval for visualizing alignment of spike times. Bottom panel shows the PSTH corresponding to the middle panel.

C. Left panel, Comparison of first-lick aligned versus spout offset aligned spike times in pre-stimulus excited neurons. Left panel shows scatter plot of maximum firing rates in first-lick aligned versus spout onset aligned PSTH's. Each data point represents the session average of one

pre-stimulus excited neuron. The right panel shows the histogram of spike distances to first lick (in blue) and spout-offset (in red) from all pre-stimulus excited neurons.

2.5. Pre-stimulus Modulations Cannot Be Accounted By Mouth Movements

Next, we performed a series of analyses aimed at understanding the behavioral correlates of pre-stimulus modulations. First, we investigated whether pre-stimulus modulations could be associated with mouth movements. It has been shown that, in addition to mouth movements during consummatory behavior, mice can move their mouth spontaneously or in anticipation of expected fluid [21, 22]. To study the possible correlations between mouth-movements and activity of GC neurons, we analyzed video recordings of the orofacial region for 124/223 units. The animal's unobstructed mouth region was filmed at 30 Hz; the recorded sessions were synchronized with neural recordings (CinePlex System, Plexon) and analyzed using custom-written software [22, 23]. For each session we defined a region of interest surrounding the mouth area (excluding the nose and the whiskers as shown in Figure 11A, left panel, white rectangle outlining the mouth) and analyzed frame to frame changes in pixel intensity within this region of interest to quantify mouth movements (see methods and [23]). The accuracy of video analysis of mouth movements was confirmed by comparing it with lick detection via a lickometer. As shown in the representative examples in Figure 11A, traces obtained from mouth movement analysis (middle trace) captured the licking activity (top trace). In addition to large licking movements, video analysis allowed us to capture small mouth movements that occurred when the spout (along with the lickometer) was in its retracted position.

Upon validating the video analysis, we compared the time course of pre-stimulus modulated population activity with that of mouth-movement activity. Figure 11B shows the population average of pre-stimulus excited neurons (in blue) and population average of pre-stimulus inhibited neurons (in red) overlaid with average of mouth movement signals recorded from the corresponding sessions (in black). Visual inspection of the traces suggests that the average neural activity may precede the average onset of mouth movements.

To quantify the correlation between mouth movements and GC neural activity on a cell-by-cell basis, and to assess the temporal relationship between the two signals, we performed a trial by trial cross correlation analysis. For this analysis, we focused on baseline spiking activity and mouth movements (3 second duration), and not on the pre-stimulus period (i.e. 500ms before the first-lick). This approach allowed us to achieve more statistical power by analyzing longer segments of data. In addition, analysis of baseline activity allowed us to prevent the detection of

spurious correlations that may result from analyzing signals aligned to common experimental triggers.

This analysis revealed that 63% (51/82) of the pre-stimulus modulated neurons (with mouth movement data) show significant cross-correlations with mouth movements (Figure 11C, left panel). Neurons with significant cross-correlations display both positive (31%, 25/82) and negative correlations with mouth movements (32%, 26/82). Next, we quantified the temporal relationship between mouth movement and neural activity in pre-stimulus modulated neurons with significant cross-correlations. The middle panel of Figure 11C shows the heat map of cross correlations where each row is the normalized session average of cross-correlations from one neuron-mouth movement pair. In each row, the lightest color corresponds to the peak of the cross-correlation. The heat map reveals that these peaks occur at widely ranging lag points. Classification of cross-correlations according to where the peak occurs, shows that 57% (29/51) of neurons display broad cross-correlation peaks around lag = 0, 33% (17/51) of neurons show spiking activity preceding mouth movements, and lastly 10% (5/51) of neurons show mouth movements preceding neural activity.

Overall, these results reveal that not all pre-stimulus modulated neurons are correlated with movements. More importantly, in the population of neurons whose activity is significantly correlated with mouth movement, the temporal relationship between spiking and movement is widely varying. Within this population, most neurons show broad cross-correlations (29/51) where neither one of the signals is clearly preceding the other. In addition, when a signal is preceding, it is more frequently the neural activity preceding the mouth movements (17/51), compared to the cases in which mouth movements precede spiking activity (5/51).

These results suggest that pre-stimulus modulations cannot simply be accounted by early mouth-movements acting as a sensory signal and driving the neural activity in GC. The lack of correlations in 37% pre-stimulus modulated neurons and the wide ranging temporal associations in those neurons with significant correlations suggests that the observed pre-stimulus modulations may be explained by additional sensorimotor, anticipatory and attentional signals.

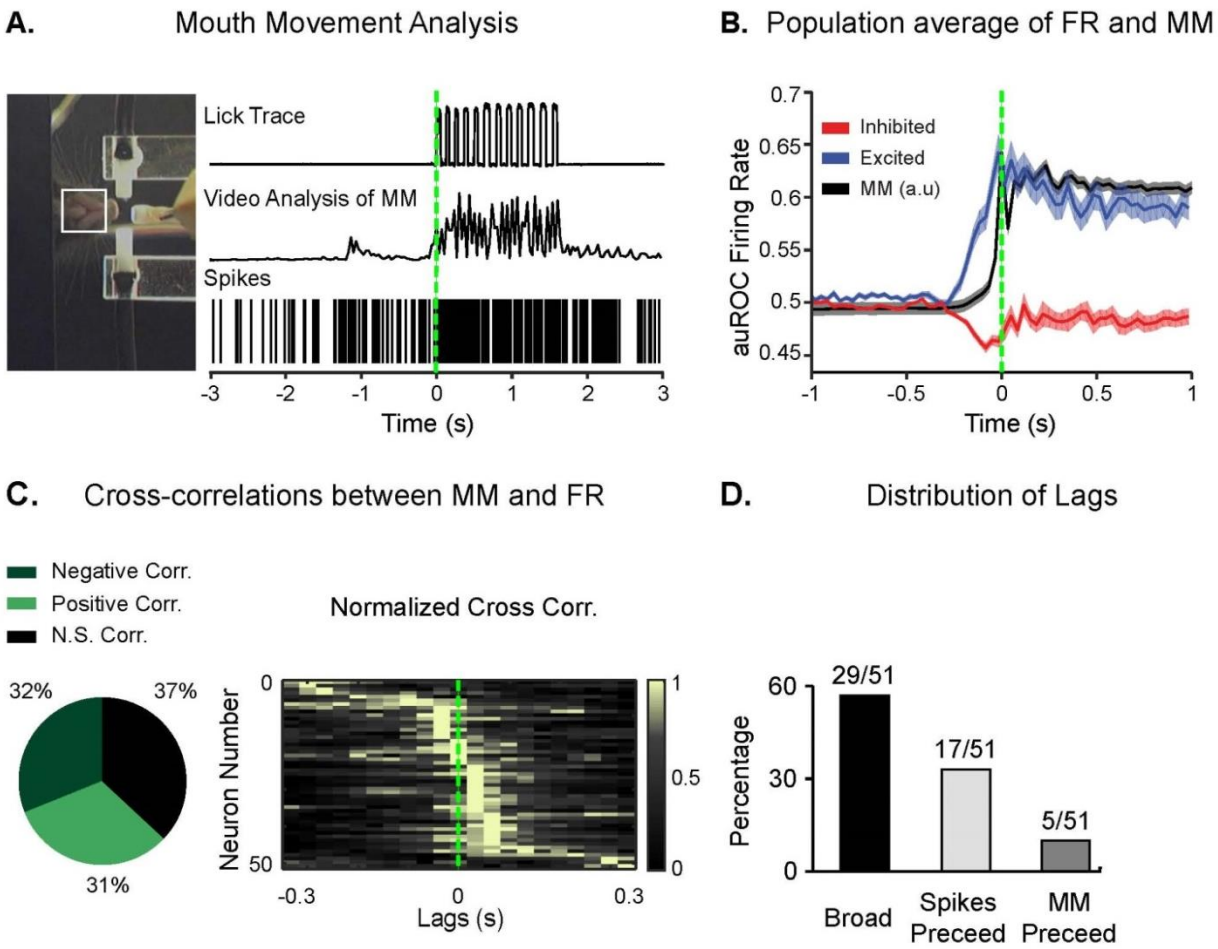

Figure 11. Mouth Movement and Firing Rate Association for Pre-Stimulus Modulated Neurons

A. Mouth movement analysis. Still image taken from a video recording during a recording session . White triangle shows the region of interest for mouth movement analysis. Right panel, analog lick signal (top), mouth movement trace extracted by the video analysis (middle) and spikes (bottom) from a representative trial.

B. Population average of firing rate and mouth movement in pre-stimulus responsive neurons. auRoc normalized population PSTH for pre-stimulus excited neurons (in blue) and pre-stimulus inhibited neurons(in red) are shown. Shadings represent SEM. Mouth movement signals from the corresponding sessions were averaged, rescaled and overlaid to visualize the relative time-course of MM and FR in the pre-stimulus epoch.

C. Pie chart shows the distribution of significant and non-significant MM-FR cross correlations in all pre-stimulus modulated neurons. Right panel shows heat map of normalized cross-correlations. For each pre-stimulus responsive neuron, the single trial cross-correlation values were averaged across all trials of the session and normalized to a [0-1] value range. Neurons were sorted in descending order by the lag of peak normalized cross correlation.

D. Distribution of lags for all pre-stimulus modulated neurons that show a significant cross correlation with mouth movement.

2.6. Active Sensing Recruits Majority of the Gustatory Cortex Neurons

We next investigated the firing rate dynamics upon animals' contact with the gustatory stimulus. Each neuron in the data set was classified as either stimulus responsive or non-stimulus responsive based on the presence or absence of significant changes from baseline firing rates in the stimulus evoked epoch (defined as the 500 ms interval between the tongue's contact with the solution and the rinse, all trial types included, see *Methods* for details).

This analysis revealed that the great majority (88%, 197/223) of neurons in GC is responsive within the first 500 ms. Specifically, deep layer neurons show greater percentage (94%, 138/147) of stimulus responsive neurons compared to superficial layer neurons (78%, 59/76) and inhibitory neurons show greater percentage of stimulus responsive neurons (96%,49/51) compared to pyramidal neurons (86%, 148/172) (both $p< 0.05$,Chi-Square test). Across all four categories where DP neurons show 92% (93/101) and SI neurons show 80% (4/5) percentage of stimulus responsive neurons, DI neurons shows the highest percentage 98% (45/46), with SP neurons showing the lowest percentage (77%, 55/71) of stimulus responsive neurons ($p < 0.01$, Chi-Square test). Next, for each category of neurons, we investigated the relative percentage of stimulus-excited versus stimulus inhibited neurons. Across all cell categories, a greater percentage of stimulus responses were excitatory. (DP: 77%, DI: 87%, SP: 60%, SI: 100%) compared to inhibitory (DP: 23%, DI: 13%, SP: 40%, SI: 0%). While the majority of stimulus modulations were excitatory for all cell categories, the relative distribution of excitatory versus inhibitory stimulus modulations was significantly different across categories ($p< 0.05$, Chi-Square test) with SP neurons showing higher inhibitory stimulus modulations compared to the other cell categories.

To visualize the firing rate patterns of stimulus responsive neurons we plotted the population PSTHs for stimulus excited and stimulus inhibited neurons within each cell category (as shown in Figure 12). As the population PSTHs demonstrate, stimulus inhibited DP neurons

show higher baseline firing rates (6.9 ± 1.7 Hz) compared to stimulus excited DP neurons (3 ± 0.5 Hz), ($p < 0.001$, Wilcoxon rank sum test). Interestingly, the opposite trend was revealed for DI neurons; stimulus excited DI neurons showed higher baseline firing rates (14.2 Hz ± 1.8 Hz) compared to stimulus inhibited DI neurons (4.8 ± 1.6 Hz) (ns, post-hoc analysis for the observed effect size reveals that the sample sizes do not grant enough power, 60%). This pattern suggests that, for both DP and DI neurons, distinct functional response properties might map onto neurons with distinct baseline firing rate profiles. Finally, the population PSTHs of stimulus excited superficial layer neurons (SP and SI) revealed strong rhythmic firing rate patterns during the stimulus evoked period.

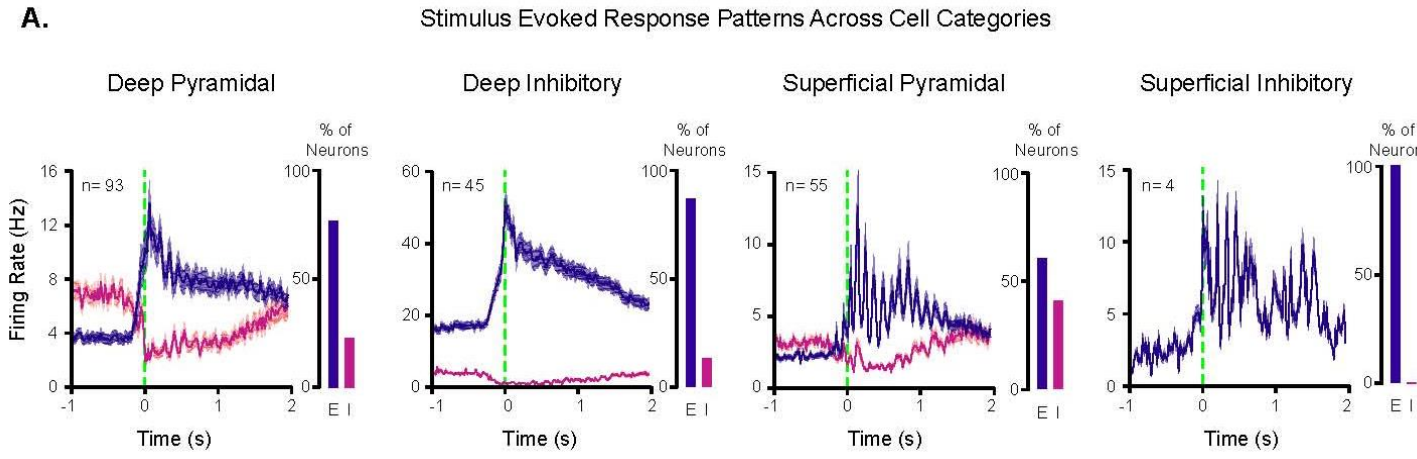

Figure 12. Distinct Stimulus Evoked Dynamics across Gustatory Cortex Neurons

A. Stimulus evoked response dynamics across categories. For each category, population PSTHs (20 ms bin size) of stimulus excited (in purple) and stimulus inhibited neurons (in magenta) are shown. Insets show the total number of stimulus responsive neurons for each category. The bar graphs show the relative percentage of stimulus excited and stimulus inhibited neurons for each cell category.

2.7. Pyramidal Neurons Display Strong Rhythmic Modulation in Stimulus Evoked Period

Population PSTHs of stimulus excited neurons revealed rhythmic firing rate patterns during the stimulus evoked period. We analyzed rhythmicity at the single neuron level by computing the power spectrum within the 1 second interval following the first-lick in lick warped PSTHs. We classified neurons as showing rhythmic activity if the power spectrum had a peak in the 6-10 Hz range and if the peak was at least 2 standard deviations greater than the median signal (see *Methods, Rhythmic Modulation of Firing Rate in Stimulus Evoked Epoch*). Using this criterion, 44% of neurons in GC (99/223) showed rhythmic activity in the stimulus-evoked epoch. The prevalence of rhythmic activity was different across cell categories where 53% (54/101) of DP neurons, 28% (13/46) DI neurons, 44% (31/71) of SP neurons and 20% (1/5) of SI neurons showed rhythmic activity ($p< 0.02$, Chi-Square test).

Next, we created lick-warped rasters to study the phase relationship between spikes and licking. For each neuron, we computed the position of spikes with respect to the lick cycle they occurred in (see *Methods, Spike Phase Consistency*). Using this method, spike times that were previously defined in seconds with respect to the onset of the first lick were redefined as positions (in radians) within the corresponding lick cycle. Figure 13A shows four representative neurons whose first-lick aligned rasters and PSTHs reveal rhythmic activity. While the rhythmicity is evident from the first-lick aligned plots, the corresponding lick warped raster plots and the rose plots give further information about the phase and the precision with which spikes occur within the lick cycles. Lick warped raster plots of representative DP and SP neurons illustrate the case in which all the spikes in the stimulus-evoked epoch occur consistently at a specific phase of the lick cycle across consecutive licks and trials. The corresponding rose plots of DP and SP neurons verify this observation; distribution of all spike phases (within the first seven lick cycles) occurred exclusively in a narrow phase-range with small variability. Interestingly, while first-lick aligned rasters and PSTHs of representative SI and DI neurons also show clear rhythmic activity, the distribution of spike-phases in the lick warped data illustrates that, in contrast with the representative SP and DP neurons, the position of spikes are distributed more broadly across the possible phase space.

For each neuron, we quantified the extent to which spikes occur preferentially at specific phases of the lick cycle by using the Spike Phase Consistency measure (see *Methods, Spike Phase Consistency*). Using this method, neurons whose spikes are positioned uniformly across the lick cycle have small spike phase consistency values, whereas neurons whose spikes cluster at particular phases of the lick cycle have high spike phase consistency values. Figure 13B displays the spike phase consistency distributions for each cell category. We found that spike phase consistency is different across cell categories ($p < 0.001$, Kruskal Wallis test), (mean ± sem for each cell category; DP: 0.73 ± 0.04, DI: 0.49 ± 0.04, SP: 0.74 ± 0.05, SI: 0.58 ± 0.15). Furthermore, post-hoc multiple comparisons across categories revealed that both DP and SP

neurons show significantly higher spike-phase consistency compared to DI neurons (for both; $p < 0.001$, post-hoc multiple comparisons with Bonferroni correction) while the DP and SP neurons are not significantly different from each other.

Next, we quantified the extent to which a neuron emits consistent number of spikes across lick-bins (i.e., single lick cycle of a single trial) using the Spike Count Consistency measure (see *Methods, Spike Count Consistency*). According to this measure, neurons that emit similar number of spikes across lick-bins have higher Spike Count Consistency values compared to neurons that emit highly variable number of spikes across lick-bins. Figure 13C shows the distribution of Spike Count Consistency measures for all four cell categories. We found that the average spike count consistency measures are different across cell categories ($p< 0.001$, Kruskal Wallis test), (mean ± sem for each cell category; DP: 0.985 ± 0.0008, DI: 0.990 ± 0.001, SP: 0.978 ± 0.001, SI: 0.980 ± 0.005). DI neurons have higher spike count consistency compared to both DP and SP neurons (for both; $p< 0.001$, post-hoc multiple comparisons with Bonferroni correction). Interestingly, we found that DP neurons show higher spike count consistency compared to SP neurons ($p < 0.001$, post-hoc multiple comparisons with Bonferroni correction).

Finally, we investigated, as shown in Figure 13D, how neurons are clustered according to these two independent measures (spike phase and spike count consistency) and whether there were differences in the clustering patterns across cell categories. For all cell categories, majority of neurons occupy the top left quadrant. These neurons, while maintaining high spike count consistency across lick bins, do not show phase preference in their spiking behavior. Activities of neurons with these characteristics are not patterned by lick cycles. Neurons in the top right portion of the scatter plots have high spike count consistency in addition to high spike phase consistency. Spiking patterns of neurons in this quadrant appear indistinguishable across lick-bins as the number and position of spikes in a given lick-bin are very similar to that of others across lick cycles and trials. We observed that a greater proportion of pyramidal neurons occupy this quadrant compared to inhibitory neurons and furthermore a greater percentage of SP neurons occupy this quadrant compared to DP neurons. This suggests that a tightly phase locked and consistent spiking pattern, as the one shown by the representative SP neuron in Figure 8A, is more likely to be observed among SP and to some extent in DP neurons. While some neurons with high spike phase consistency also display high spike count consistency across lick-bins as described above, some SP neurons (in the lower portion of the scatter plot) can display spike phase consistency without spike count consistency. The spiking behaviors of such neurons are characterized by spikes emitted preferentially at a specific phase of the lick cycle but the occurrence and the number of such spikes is highly variable across lick cycles and trials. Overall, Figure 8D reveals that SP neurons show greater diversity in their spiking behavior during licking.

In summary, these results show that neurons in GC can display rhythmic activity during licking and in a subset of these neurons, spikes occur exclusively at specific phases of the lick cycle. In addition, our results show that while DI neurons show greater spike count consistency across lick-bins compared to SP and DP neurons, pyramidal neurons on the other hand display greater spike-phase consistency compared to DI neurons.

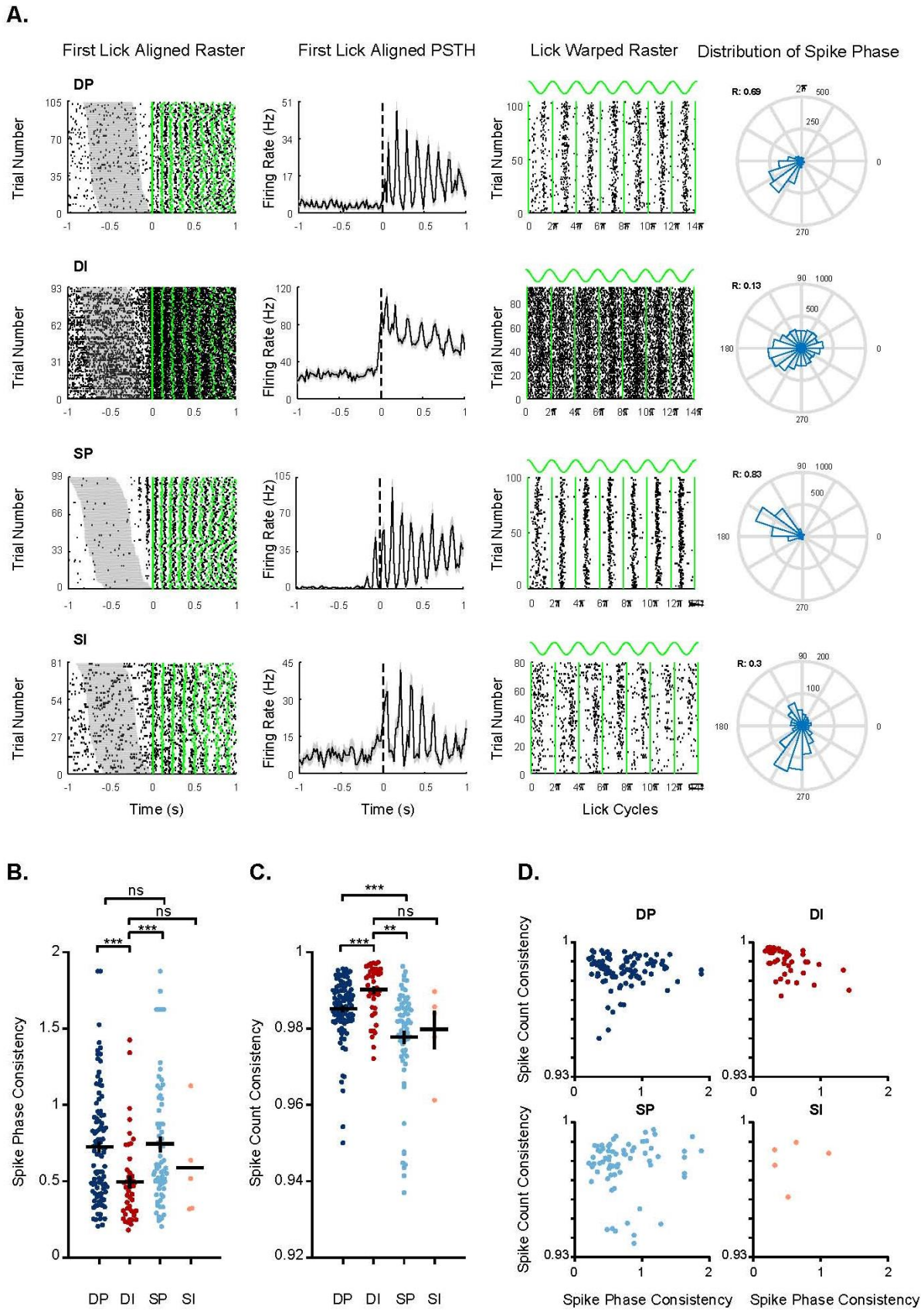
A.
First Lick Aligned Raster
First Lick Aligned PSTH
Lick Warped Raster
Distribution of Spike Phase
DP
DI
SP
SI
Trial Number
Firing Rate (Hz)
Time (s)
Lick Cycles
R: 0.69
R: 0.13
R: 0.83
R: 0.3
B.
Spike Phase Consistency
C.
Spike Count Consistency
D.
Spike Count Consistency
Spike Phase Consistency
ns
***
**

Figure 13. Licking Patterns the Activity of Gustatory Cortex Neurons in a Cell Category Specific Way

A. Representative examples of neurons with rhythmic activity. Going from top to bottom, each row of the panel shows one representative neuron selected from DP, DI, SP and SI cell categories respectively. For each representative neuron, the first column shows the raster plot aligned to the first-lick (at time =0) where black ticks represent the spikes and green ticks represent the licks. The second column shows the first-lick aligned PSTH in the same time-scale. Third column of the panel shows lick-warped raster plots, where the relative position of spikes within the first seven lick-cycles are plotted in radians. Vertical green lines represent the beginning and end of the lick cycles. The last column shows the phase distribution of all spikes that occur within the first seven lick cycles on a rose plot. The R-value next to the rose plot shows the mean vector length of the circular distribution. The values next to the inner and outer circles of the rose plot indicate the number of observations.

B. Spike phase consistency distributions for each cell category. For each neuron, a spike phase consistency measure was computed to assess the degree to which the spikes occurred at a specific phase of the lick cycle. Mean (horizontal black line) and standard error of the mean (vertical black line) of spike phase consistency is shown for each category of neurons. The group means are compared using Kruskal-Wallis test followed with multiple comparisons using Bonferroni corrections (*** indicates $p < 0.001$, ** indicates $p<0.01$).

C. Spike count consistency distributions for each cell category. Spike count consistency was measured for each neuron to assess the degree to which the number of spikes elicited by a lick were consistent across lick cycles and trials. Mean (horizontal black line) and standard error of the mean (vertical black line) of spike phase consistency is shown for each category of neurons. The statistical procedures are same as described for panel B.

D. Scatter plots of spike count versus spike phase consistency measures for each cell category.

2.8. Gustatory Cortex Neurons Encode Taste in Rapid Timescales and Chemosensitivity is Biased to Deep Layer Pyramidal Neurons

To assess the chemosensitivity of single neurons, lick warped rasters and PSTHs were created for each taste response category. Neurons whose response patterns varied across different tastants were classified as chemosensitive neurons (see *Methods, Taste Coding Analysis*). Only the lick cycles occurring prior to the rinse were included in the analysis. Figure 14A and 14B show two representative, chemosensitive single neurons. The representative neuron in Figure 14A shows higher firing rates to salt and this differential response begins within the first lick cycle. The representative neuron in Figure 14B responds to all five taste stimuli with changes in firing rate; interestingly, citric acid and salt elicit inhibitory responses whereas water, sucrose and quinine elicit temporally distinct excitatory responses. The differential responses emerge within the first two lick cycles. Overall, 31% of GC neurons (69/223), show chemosensitivity. As illustrated in Figure 14C, the percentage of neurons that display chemosensitivity varies across cell categories ($p<0.05$, Chi-Square test) with 40% DP, 24% DI, 23% SP and 20% SI neurons showing chemosensitivity. This analysis shows that a greater percentage of DP neurons show chemosensitivity compared to other categories. Next, to assess the breadth of tuning, we investigated the number of different tastants a neuron responded to. For each neuron that was classified as chemosensitive, the number of tastants that showed a differential response from water was identified using post-hoc multiple comparisons with Bonferroni correction. The results of this analysis for each cell category are illustrated in Figure 14D. For deep layer categories (DP and DI), the majority of the neurons differentiate a single tastant, with a small percentage differentiating two and three tastants from water. SP neurons on the other hand display a larger percentage of neurons that can differentiate three tastants apart from water.

Overall, these results show that GC neurons display taste specific responses within the first 500 ms after a single drop of taste delivery. Furthermore, the DP neurons display the greatest percentage of chemosensitive neurons with SP neurons showing broader tuning properties compared to DP and DI neurons.

2.9. Convergence of Different Functional Features in Gustatory Cortex Neurons

Thus far, we have demonstrated three distinct functional phenemena in GC neurons; pre-stimulus modulations, lick modulations and taste specific modulations. We next investigated whether these distinct features are represented by different neurons or whether they can converge on the same single neurons. Representative examples of neurons that demonstrate convergence of two or three features based on the previously described criteria are plotted in Figure 15A-D. To visualize pre-stimulus modulations, all trial types were collected and aligned to the first lick onset, to visualize lick modulations, lick-warped raster and PSTHs for the first five lick cyles

were are plotted for all trials. Finally, to visualize the taste specific modulations, the middle panel is replicated with the raster and PSTHs color coded by taste trial type. Figure 15A, illustrates a neuron that displays inhibitory pre-stimulus modulations, lick modulation and taste specific responses to quinine (in green). Figure 15B, illustrates a neuron that displays excitatory prestimulus modulations, no lick rytmicity and salt specific activity. Figure 15C, illustrates a neuron that doesn't display prestimulus modulations but has lick rhtymicity and citric acid specific activity and Figure 15D illustrates a neuron that displays excitatory prestimulus activity, lick rhtymicity but no taste specific activity.

These representative examples illustrate that the distinct functional features can co-occur in single GC neurons. Indeed, at the population level, 41% (92/223) of all recorded neurons display more than one type of modulation, whereas 44% (98/223) of all neurons display a single feature. The distribution of functional convergence across features can be seen in Figure 16. Overall, these results show while single GC neurons can exclusively display a specific functional feature, they can also display more than one feature.

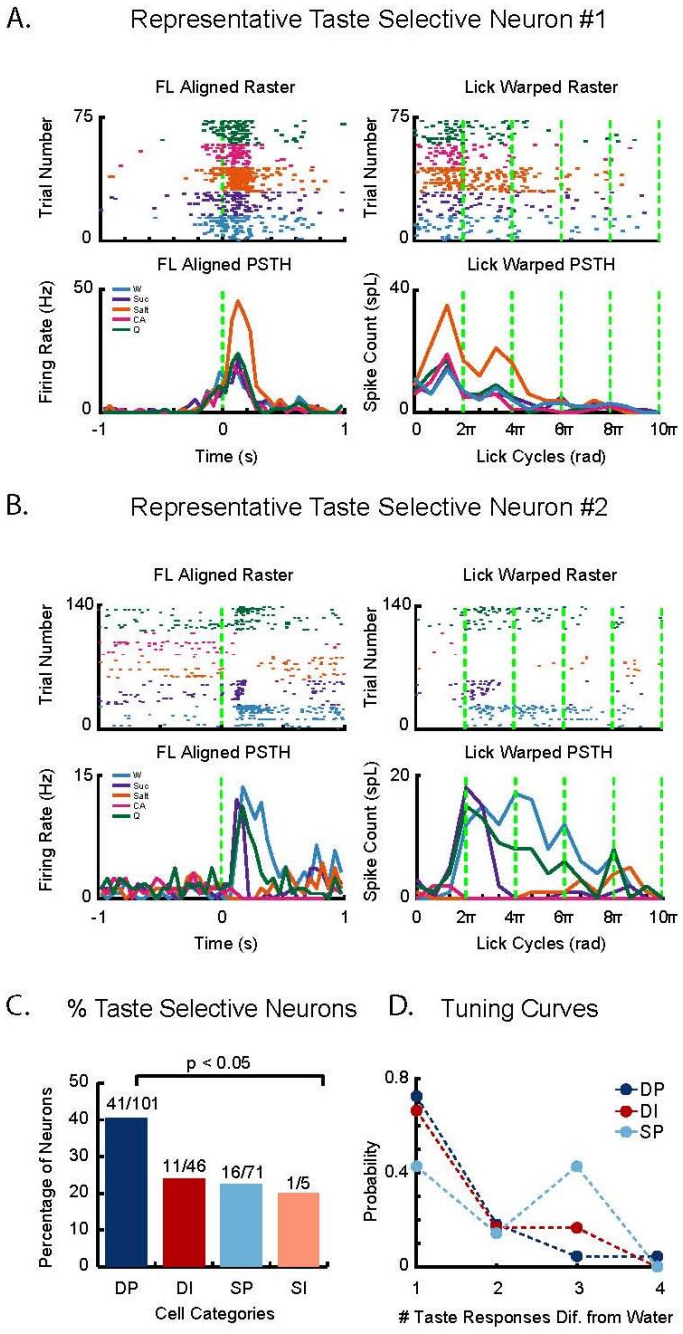

Figure 14. Taste Coding in Gustatory Cortex

A. Representative taste selective GC neuron. Left panel shows the first lick aligned raster (top) and PSTH (bottom) color coded for each tastant as shown in the inset. Right panel shows the lick cycle warped activity of the same neuron with the raster (top) and PSTH (bottom). The representative neuron responds to all taste stimuli with an increase in firing rate above baseline and its activity is selective for salt.

B. Representative taste selective GC neuron. Panels organized same as in A. The neuron responds to three taste stimuli with increases in firing rate and to two taste stimuli with

decreases in firing rate. The excitatory responses display taste specific time varying changes in firing rate.

C. Percentage of taste selective neurons in each cell category. Taste selectivity varies across categories with DP neurons showing the highest percentage of taste selective neurons.

D. Breadth of tuning across cell categories. For each category, the probability of observing neurons that respond to 1,2,3, or 4 stimuli differently than water are plotted.

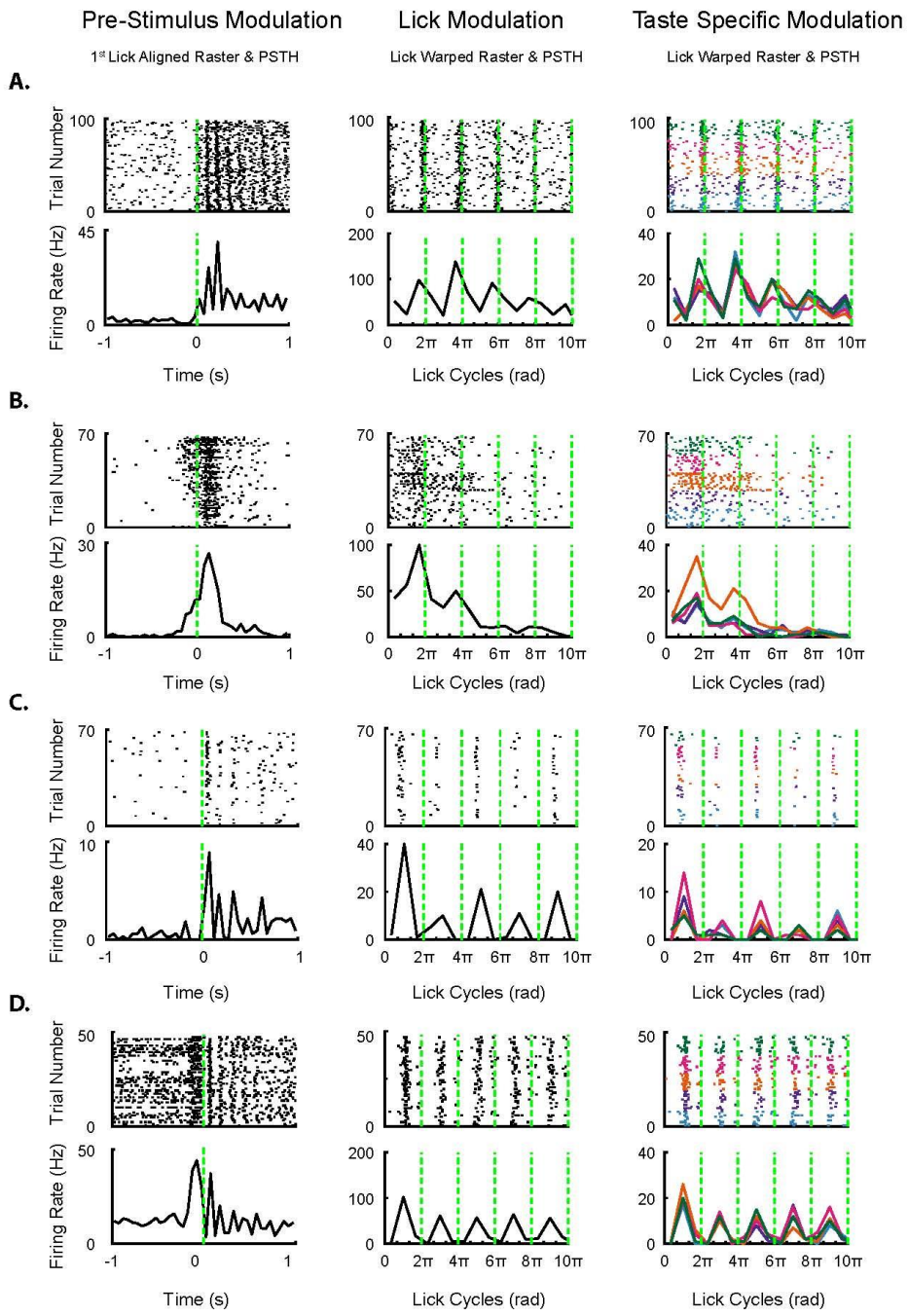

Figure 15. Convergence of Different Phenomena on Single GC Neurons

Four representative neurons displaying convergence of distinct features are plotted. For A-D, left panels show the raster (top) and PSTH (bottom) of first-lick aligned activity for all trial types. The modulation of activity prior to time 0 indicates pre-stimulus modulation. Middle panels show the lick warped raster (top) and PSTH (bottom) for the first five lick cycles occurring prior to the rinse. 0 radians on the x-axis indicates the onset of the first lick and

consecutive licks are marked as green dashed lines. All trial types are grouped to visualize presence of rhythmic activity. Right panels show the same lick warped raster and PSTH as in the middle plots but the activity is color coded according to taste trial type to visualize taste specific activity.

A. Representative example of single GC neuron that displays inhibitory pre-stimulus modulation, lick rhythmic activity and taste specific activity for quinine (in green).
B. Representative example of single GC neuron that displays excitatory pre-stimulus modulation, no lick rhythmicity and salt selective activity.
C. Representative example of single GC neuron that displays no pre-stimulus modulation, lick rhythmicity and citric acid selective responses.
D. Representative example of single GC neuron that displays excitatory pre-stimulus modulation, lick rhythmicity and no taste selective activity.

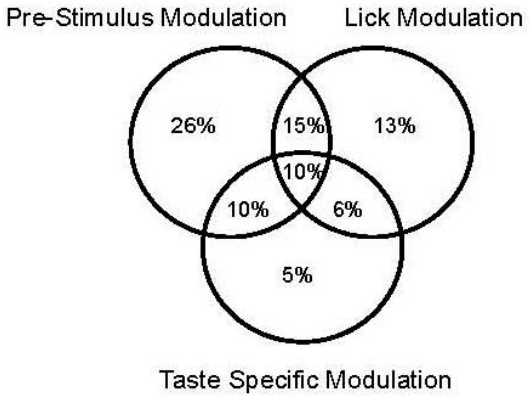

Figure 16. Convergence of Functions

Diagram illustrates the percentage of neurons that display each type of functional convergence. 85% (190/223) neurons display at least one type of modulation. 15% (33/223) of neurons do not show any type of modulation and are excluded from the diagram.

Chapter 3

General Discussion

Studies in visual, somatosensory and auditory primary cortices have elucidated that neurons belonging to different layers and cell types have distinct upstream connectivity patterns that shape their functional properties. The interactions among the neurons with distinct functional properties give rise to the complex computations performed in these regions [1, 2]. Despite the importance of studying the functional properties of neurons belonging to distinct layers and cell types for understanding the mechanisms of cortical computations, no study to date has addressed this question in gustatory cortex. My dissertation work aimed at addressing this gap in the literature and revealed important new findings regarding the functional properties of gustatory cortex neurons belonging to different layers and cell types.

3.1. Baseline Firing Rate Differences in Gustatory Cortex Microcircuit

Electrophysiological studies in primary sensory cortices have shown that neurons within different cell categories display distinct firing rates at baseline and stimulus evoked conditions [1, 2, 57]. To assess whether similar distinctions exist within GC neurons, I have investigated the firing rates of excitatory and inhibitory neurons in deep and superficial layers of gustatory cortex. Baseline was defined as the 1 second interval prior to the trial's beginning where there were no overt stimuli. The results revealed that the baseline firing rates were significantly different across cell categories, with deep layer inhibitory neurons (DI) displaying higher firing rates at 13 Hz compared to deep layer pyramidal neurons (DP), superficial layer pyramidal neurons (SP) and superficial layer inhibitory neurons (SI). There were no significant differences across the DP, SP and SI whose mean baseline firing rates ranged from 0.7 Hz to 3Hz. Stimulus evoked activity was assessed based on the 500 ms interval between the first-lick and the rinse. Average firing rates in the stimulus-evoked epoch were also significantly different across cell categories with DI neurons showing the highest average firing rate at 36 Hz. Interestingly, while DP, SP and SI neurons showed similar firing rates at baseline, the differences in their activity became prominent in the stimulus evoked epoch with DP neurons showing significantly higher firing rates than SP neurons. These results suggest that there are indeed differences in the firing rates of GC neurons both based on laminar and cell type classification, and these differences are amplified during the stimulus-evoked state. It is possible that the observed differences in firing rates are a reflection of the differences in intrinsic properties and/or differences in upstream connectivity across categories. While both of those properties might differ across categories, it is more likely that the differences observed between DP and SP neurons during the stimulus-evoked epoch reflects their upstream connectivity and the resulting synaptic inputs.

These results are consistent with findings from other primary sensory cortices where neurons in superficial layers were found to fire much more sparsely than deep layer neurons [6, 17, 57]. This was attributed to the differing contribution of inhibitory input that deep versus superficial layers receive. Indeed, *in vitro* and *in vivo* studies have shown that the superficial layer neurons are under greater inhibitory tone compared to deeper layers [10]. The strong inhibitory inputs onto the superficial layer neurons counteract the synaptic excitation and consequently the membrane potential rarely reaches spike threshold. Studies in other sensory cortices have also reported that inhibitory neurons display higher firing rates compared to excitatory neurons [58]. It is important to note that not all inhibitory neurons display high firing rates and the spontaneous and evoked firing rates can show distinctions across inhibitory neuron subtypes [34].

It is worth noting that we have recorded from very few putative inhibitory neurons in the superficial layers. In the deep layers, the inhibitory neurons constituted 40% of the total isolated units whereas in the superficial layers they only made up 7% of the isolated units. The first possible explanation is that there are fewer inhibitory neurons in the superficial layers of GC. The second possibility is that the types of inhibitory neurons that are present in the superficial layers of GC do not show narrow waveforms and there for cannot be classified with our method. The in situ hybridization data available in the Allen Brain Atlas illustrate that inhibitory neurons indeed show laminar specific distribution patterns in GC with VIP neurons predominantly occupying superficial layers and PV neurons showing denser distribution in the deeper layers. This layer specific distribution has also been observed in primary somatosensory cortex where PV neurons are concentrated in L4-L6 and the 5HT3a neurons (which include the VIP neurons) are concentrated in L1-L3[34]. While there is no one-to-one mapping between the molecular expression and electrophysiological properties of inhibitory neurons, PV neurons have mostly been shown to display fast-spiking activity with narrow waveforms. Furthermore, the spontaneous and stimulus evoked firing rates of PV neurons have been shown to be significantly higher than that of VIP neurons in auditory cortex of mice. It is possible that the lower firing rate of VIP neurons might lead to a sampling bias where they are less likely to be detected and sorted in extracellular recording configurations. The basis for low inhibitory neuron sampling in the superficial layers would need to be further investigated using immunohistochemistry and slice electrophysiology techniques.

3.2. Pre-stimulus Modulations in Gustatory Cortex

Cue responses

Neurons in gustatory cortex have been shown to display modulations to cues that predict taste delivery [22, 23, 121]. While the experimental paradigm presented in this dissertation was not explicitly designed to study such cue responses, the trials did include an auditory cue prior to the spout movement. To assess whether GC neurons displayed cue responses in this paradigm, the trials were aligned to the cue and firing rates in the 500 ms following the cue were compared to the baseline firing rates. Neurons that showed significant modulations as assessed by a Mann-Whitney U test were classified as cue-responsive neurons. This analysis revealed that 10% of GC neurons show cue responses and the magnitude of these modulations are smaller than previously described. Furthermore, there are no significant differences in percentage of cue-responsive neurons across cell categories. Previously published work from our lab has shown that in rats implanted with intraoral cannulas (IOC), auditory cues predicting delivery of taste stimuli can elicit cue-responses in 20% of GC neurons and olfactory cues can evoke responses in 40% of GC neurons [21-23]. The differences between the work presented here and the previous reports on the percentage of cue-responsive neurons are likely due to the differences in experimental designs and preparations. The high cue-percentages reported in previous work were observed in rats implanted with IOCs, where the taste stimuli were directly delivered to animal's mouth either following a cue (classical conditioning) or following a lever-press after the cue (operant conditioning). In addition, the average time between the cue onset and taste delivery was shorter in these paradigms. In contrast, in the experimental paradigm presented herein, the auditory cue indicates the movement of the spout, and the taste stimulus is conditional upon the animal initiating a lick once the spout is in position. I argue that the presence of an intermediate step (the spout movement) between the cue and the taste delivery decreases the saliency of the auditory cue resulting in fewer cue-responses. Indeed, it has been shown that the percentage of cue-responsive neurons in GC increases as the cue acquires higher saliency through learning [21]. It is also possible that the cue and the spout movement become a compound cue and the firing rate modulations do not occur with the cue onset, but rather with spout movement. This opens up the question of whether the spout movement, either the movement onset or offset can act as a cue that elicits responses in GC neurons which will be addressed in the subsequent sections.

Pre-stimulus modulations

Aligning the neural activity to the first-lick onset and plotting the population activity as a heat-map illustrated that, in a subset of neurons, firing rate modulations begin prior to animals' contact with the taste solution. Following this observation, each neuron's activity in the pre-stimulus epoch (500 ms prior to first-lick) was classified as either pre-stimulus modulated or non-pre-stimulus modulated depending on the presence or absence of significant changes from baseline firing rates. This analysis revealed that 60% of GC neurons display pre-stimulus modulations and that these modulations can be excitatory (38%) or inhibitory (22%). While pre-

stimulus modulations were observed in all cell categories, DI neurons showed the highest percentage (89%) of pre-stimulus modulated neurons and SP neurons showed the lowest percentage of pre-stimulus modulations (41%). In addition to the differences in percentage of pre-stimulus modulated neurons, the types of predominant pre-stimulus modulations were also distinct across categories. DP neurons showed excitatory and inhibitory pre-stimulus modulations with a small bias towards excitatory modulations. SP neurons also showed both type of pre-stimulus modulations with a small bias towards inhibitory modulations. DI neurons, on the other hand showed a very strong bias towards excitatory pre-stimulus modulations with only 15% of the modulations being inhibitory. SI neurons, although a very small sample size, displayed the same trend with only excitatory pre-stimulus modulations. Furthermore, pre-stimulus excited DI neurons had higher baseline firing rates compared pre-stimulus inhibited DI neurons.

Taken together, these results suggest that pre-stimulus modulations occur predominantly in the deep layers of GC leading to excitatory responses in great majority of inhibitory neurons. The small percentage of pre-stimulus inhibited DI neurons display significantly lower firing rates than the pre-stimulus excited DI neurons. It is possible that these DI neurons with distinct baseline firing rates and pre-stimulus modulations patterns correspond to genetically distinguishable subtypes of inhibitory neurons. Based on the distribution of inhibitory neurons within GC, with deep layers being constituted by PV and VIP neurons, it is possible that pre-stimulus excited neurons with high baseline firing rates correspond to PV neurons, while the low firing rate pre-stimulus inhibited neurons correspond to VIP neurons. Based on the known connectivity among inhibitory interneurons, it is possible that the pre-stimulus excitations in the DI neurons result from the disinhibition that is provided by the inhibitory modulation of the putative VIP neurons. Such a mechanism has been seen in other primary sensory cortices where the cortico-cortical inputs preferentially target VIP neurons, leading to a disinhibition in the cortical circuit [9, 10, 67, 122, 123].

Pre-stimulus modulations are aligned to the first-lick

We investigated whether the observed pre-stimulus modulations are associated with the spout movement either through the spout acquiring a predictive value, or through the spout acting as a sensory stimulus. The duration of the spout movement (i.e. the interval between the spout movement's onset and offset) was fixed for a given session and therefor aligning the trials to the spout onset could inform us about possible modulations that occur at any point along the spout movement. While the spout duration was fixed throughout the session, the interval between the spout onset and first-lick initiation was variable across trials. We exploited this

variability in the spout onset to first-lick interval to assess whether the pre-stimulus modulations that occurred within these two events were better aligned to the one or the other event. For each pre-stimulus excited neuron, two PSTHs were created: one where trials were aligned to the onset of the spout movement and one where the trials were aligned to the onset of the first-lick. This analysis revealed that for all the pre-stimulus excited neurons in the data-set, the modulation was better aligned to the first-lick onset than the spout movement. We limited our analysis to pre-stimulus excited neurons as increases in firing rate were more robust than decreases in firing rates. I argue that the driving cause of pre-stimulus modulations are very unlikely to be different for pre-stimulus excited versus pre-stimulus inhibited neurons and therefore reason that findings from pre-stimulus excited neurons, showing that their modulation is aligned to the first-lick onset, can also be extended to pre-stimulus inhibited neurons. Overall, these results show that spout movement does not modulate activity of GC neurons and that instead pre-stimulus modulations are associated with the onset of the first-lick.

Association of pre-stimulus modulated neurons with mouth movements

I have investigated the possible behavioral correlates of pre-stimulus modulations by studying the relationship between mouth movements and spikes. This analysis was motivated by the frequent mouth movements that mice (and rats) display both spontaneously and in anticipation of taste solutions. I reasoned that since GC, as well as other nuclei along the gustatory pathway, can respond to stimulation of the oral region, the observed pre-stimulus modulations could result from the somatosensory input associated with the potential mouth movements occurring prior to the lick onset. Cross correlation analysis between mouth movements and spikes revealed that not all pre-stimulus modulated neurons display significant correlations with mouth movements and the subpopulation of neurons that do have significant correlations display complex temporal relationships where spikes precede mouth movements in majority of the cases. In a small percentage of neurons, the mouth movements precede the firing rate modulations.

Taken together, these results suggest that while GC firing rate modulations and mouth movements can co-occur, the wide temporal range of the correlations between the two signals suggests that the two phenomena might not necessarily be directly linked, but rather be related through a third variable which influences both signals independently. It is possible that the changes in arousal and/or attention lead to behavioral changes, as observed in animals moving their mouth, and to neural activity changes through neuromodulatory mechanisms. In fact, neurons in GC receive inputs from noradrenergic and cholinergic nuclei [124]. According to this view, it is possible that the pre-stimulus modulations reflect a global state change mediated by

neuromodulatory systems as animals transition from a quiet state to an active, licking state. It worth noting that, for a given pre-stimulus modulated neuron, the modulation onset is relatively invariant from trial-to-trial suggesting that the source of the modulations provides robust and rapid acting input onto the GC neurons. Another candidate source of these modulations could be subcortical or cortical regions processing motor functions. It is possible that a movement preparation signal originating from such regions could be communicated to sensory areas. However, in the retrograde tracing experiments, much to our surprise, such projections were not observed (*data not shown*), eliminating the possibility of at least a monosynaptic input from motor related regions modulating the GC activity.

In conclusion, GC neurons display layer and cell type specific modulations prior to the onset of a licking bout. Neurons in deep layers, specifically DI, show stronger pre-stimulus modulations. However, this phenomenon can be observed in all the class of neurons that we recorded from. These modulations, both excitatory and inhibitory, begin on average 200 ms prior to the first-lick onset and cannot be accounted for by spout movement or mouth movements. Given the co-occurrence of firing rate modulations with mouth movements in a subset of neurons it is possible that the observed pre-stimulus modulations are driven by neuromodulatory signals affiliated with state changes as animals prepare to begin licking. The role of these wide spread modulations, particularly the extensive recruitment of deep layer inhibitory neurons, and how they affect subsequent sensory processing would need to be investigated using loss of function experiments.

3.3. Stimulus Evoked Rhythmic Firing Rate Dynamics in Gustatory Cortex

Stimulus Modulations

We next analyzed the stimulus evoked firing rates by comparing them to baseline. This analysis revealed that the great majority of GC neurons (88%) show significant firing rate changes within the 500 ms interval following the first-lick onset. While the predominant response type was excitatory across categories, the relative prevalence of excitatory and inhibitory modulations differed across the categories with 87% of DI neurons showing excitatory responses compared to the 60% of SP neurons showing excitatory responses. Furthermore, of all the cell categories investigated, SP category showed the highest percentage of inhibitory responses in the stimulus evoked epoch. The same trend was also present in the pre-stimulus epoch where the highest percentage of inhibitory modulations was again observed in SP neurons. These results suggest that the relative strength of inhibition compared to excitation is greatest in SP neurons. This could either be explained by SP neurons receiving weaker excitatory input compared to other cell categories or by SP neurons receiving stronger inhibition compared to other cell categories with all else being equal. Given the results of in vivo whole cell patch clamp

studies in other primary sensory cortices, where SP neurons were shown to receive stronger inhibitory inputs [10], a similar phenomenon could be the cause of observed differences in GC cell categories as well. If SP neurons are indeed under stronger inhibitory tone within the circuit, it is likely that the deep layer inhibitory neurons that are extensively responsive both during the pre-stimulus and stimulus evoked epochs could be providing this inhibition.

Comparing the response dynamics of neurons that display excitatory versus inhibitory modulations within a given category revealed that these different functional responses map onto subpopulations with distinct firing rates. DP neurons with high baseline firing rates show inhibitory responses whereas DP neurons with low baseline firing rates shows excitatory responses during the stimulus evoked epoch. The opposite trend is revealed for DI category where neurons with low baseline firing rates are inhibited and neurons with high baseline firing rates are excited. Although not significant, a similar effect as the one observed with DP neurons is also present for SP neurons.

Licking patterns GC neural activity

The population PSTHs of stimulus-evoked activity revealed rhythmic patterns in our data-set. This observation prompted a further investigation into the possible rhythmic modulations in single GC neurons. Such rhythmic activity has previously been described in other nuclei along the taste pathway, as well as in GC of licking animals. These studies have reported that the rhythmic firing patterns occurred in the same frequency range as the licking frequency (6-10 Hz) [20, 117, 118, 125]. To assess whether single GC neurons displayed such rhythmic modulations in our experimental paradigm and whether there were any layer and cell type specific effects, I investigated the power spectrum of stimulus-evoked firing rates. For the analysis described in this section I used lick warped raster and PSTHs to eliminate the variability introduced by changes in lick patterns across trials and animals. Neurons were classified as showing lick related rhythmic activity if the power spectrum showed a significant peak in the 6-10 Hz range. This analysis revealed that 44% of GC neurons display rhythmic firing rates during licking with pyramidal neurons in deep and superficial layers showing higher prevalence of rhythmic activity compared to inhibitory neurons. Next set of analysis, focused on quantifying to what extent spikes occurred preferentially at specific phases of the lick-cycle. This analysis showed that overall, the spikes of DP and SP neurons are concentrated at narrow phase range of the lick-cycle whereas DI and SI neurons, despite showing rhythmic activity do not display such preferential spiking within the cycle. Furthermore, I quantified the extent to which neurons emitted similar number of spikes across lick cycles and trials. This analysis was done to differentiate between neurons that reliably emit the same number of spikes within the same phase

range across trials and lick-cycles versus the neurons that show preferential spiking within a specific phase of the lick cycle but spike very sparsely and therefor show high variability in their spike counts across lick cycles and trials. This analysis revealed that while DP neurons show consistent spike counts across lick cycles, SP neurons tend to show highly variable spike counts across lick cycles.

The role of licking for the gustatory system is analogous to the role of sniffing for the olfactory system. Licking is both a rhythmic sensory and motor act structuring the temporal pattern of the taste input as animals make rhythmic contact with solutions. Furthermore, licking also creates rhythmic somatosensory stimulation of the tongue and oral region which has previously been shown to be represented along the gustatory pathway. Given this robust influence of licking in patterning the sampling process, it is not surprising that the neural activity along the taste pathway shows rhythmic firing rate modulations [20, 82, 85, 117, 125]. The results presented in this dissertation expand on the previous findings by demonstrating that the licking induced rhythmicity of neural activity is stronger in pyramidal neurons compared to inhibitory neurons. It is most likely that this rhythmic activity is a continuation of the rhythmicity observed throughout the gustatory system in licking animals. Given how consistent the spike phase is across lick cycles and trials, this effect is likely driven by a region that provides strong and extensive input to GC such as VPMpc. It is possible that the observed difference across cell categories is a reflection of how VPMpc targets neurons within GC. If the thalamocortical projection pattern between VPMpc and GC is similar to those observed in other sensory systems [126], than I would expect VPMpc to primarily target pyramidal neurons of deep layers in GC. This projection pattern would lead to a more faithful transfer of rhythmic activity in the neurons that receive direct input from VPMpc. Neurons that either do not receive direct innervation from the source of rhythmic activity, or receive sparse innervation are more likely to display weak rhythmicity and high trial to trial variability in spike phase.

In summary, I argue that the rhythmic activity in GC is a result of ascending inputs from the gustatory pathway and the relative differences observed across cell types and lamina is a reflection of the differences in how the source of this rhythmic activity preferentially innervates the cell categories within GC.

3.4. Taste Coding in Gustatory Cortex

In this experimental paradigm, animals received one drop of taste solution which was delivered on the first lick. I investigated whether this minimal stimulation evoked taste specific

responses within GC neurons. Neurons were classified as chemosensitive based on the presence of significant differences across their responses to different taste stimuli. This criterion allowed us to exclude neurons who responded with significant changes from baseline firing rates but whose modulations were indistinguishable across different taste stimuli. Although such neurons were classified as stimulus responsive, they did not carry any taste related information and were classified as non-chemosensitive. Our results revealed that 31% of GC neurons show chemosensitive responses within the 500 ms following the contact with a single drop of taste solution. Furthermore, chemosensitivity of neurons show layer and cell type specificity with DP showing the highest percentage (40%) of chemosensitive neurons. I next investigated the breath of tuning of GC neurons, as the binary classification of chemosensitivity does not fully capture how the neurons encode taste information. In fact one of the ongoing debates on GC function is whether the taste responsive neurons are broadly tuned (i.e. responding to multiple tastes) or narrowly tuned (i.e. responding to single taste stimuli). This analysis showed that for each cell category (DP,DI,SP), most neurons differentiate one taste stimuli from water. Interestingly, the analysis revealed that a greater percentage of SP neurons can differentiate three taste stimuli from water compared to DP and DI neurons. The tuning curves observed in this data set point to narrower tuning curves than previously reported in GC [97]. This difference can be attributed to the differences in method and amount of taste delivery across the paradigm presented herein and the previous reports using intra-oral cannulas.

Overall, these results provide further support for mix of both broad and narrowly tuned neurons within GC. Contrary to the findings and theories from visual cortex where superficial neurons display increased stimulus selectivity compared to deep layers, the results from GC show superficial layers showing more broadly tuned responses.

3.5. Functional Convergence in Gustatory Cortex

Historically, a subset of studies in GC has excluded neurons that displayed licking rhythm from their analysis [19, 21, 23, 97]. The authors of these studies have argued that such neurons were somatosensory neurons and did not carry taste related information. In the work presented here, I investigated to what extent the distinct functional features described for GC could be present in single neurons. The results revealed that both pre-stimulus and lick rhythm modulated neurons could code for taste information. Furthermore, the results revealed that not pre-stimulus modulated and lick rhythm modulated neurons were only partially overlapping. This partial overlap can be interpreted as the two observations corresponding to distinct phenomena rather than manifestations of the same signal separated in time. Figure 17 shows a schematic of how the GC might represent these varying features. In the first model, all three functions are represented

by non-overlapping populations of neurons. In the revised model based on the results of this dissertation, any combination of pre-stimulus, lick, or taste related modulations can convergence on single GC neurons. Yet the fact that these three modulations do not show full overlap suggests that each phenomenon represents a stand-alone feature and not an epiphenomenon associated with one of the other two functional properties.

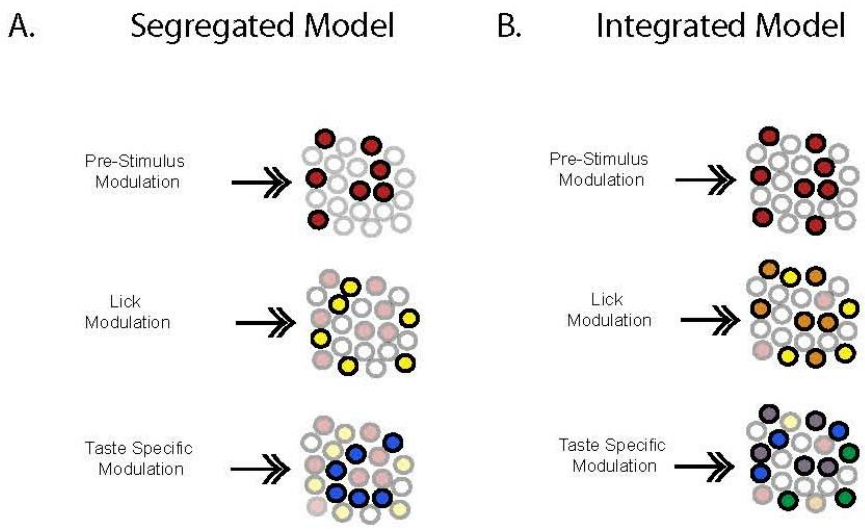

Figure 17. Model of Functional Convergence in GC

A. The schematic for the segregated model illustrates, starting with pre-stimulus modulations, how each modulation targets a different subset of neurons within GC. Each primary color corresponds to one type of functional modulation.

B. The schematic for the integrated model illustrates that each additional functional modulation can target a subset of the neurons that have previously been modulated by other phenomena in GC. The primary colors represent neurons that only show one type of functional modulation. Merged colors represent neurons that show two or three different functional modulations.

3.6. Future Directions

The work presented in this dissertation reveals that there are important distinctions between the spontaneous and stimulus evoked properties of GC neurons belonging to distinct lamina and cell types. The findings demonstrated herein provide a starting point for a more in depth circuit based analysis of GC functions. In future studies, more precise methods should be used to distinguish neurons belonging to distinct lamina and cell types. Such specificity for cell types can be obtained by combining extracellular recordings with optogenetic techniques where channel-rhodopsin (ChR) is expressed exclusively in excitatory or inhibitory neurons. Laminar

specificity can be obtained by injection of floxed ChR virus into GC of animals expressing Cre in specific layers. These approaches would be particularly useful for understanding the response properties of superficial inhibitory neurons which seem particularly elusive to our experimental approach. Furthermore, it would be particularly important to resolve the differences between neurons in L4-L6 as these neurons correspond to different stages in the cortical processing. While these methods can provide greater certainty about the identity of the recorded neurons, they still do not resolve the conceptual complexity introduced by the changing laminar organization of GC along the dorsal-ventral axis.

To understand the basis of low firing rates and responsiveness in superficial layers, experiments implementing in vivo patch clamp can be pursued to study the synaptic inputs onto these neurons. Being able to isolate the excitatory and inhibitory components of their synaptic inputs would inform us how the circuit interacts with the superficial layer neurons.

The next interesting question to pursue would be to understand the source of pre-stimulus modulations. This question can be addressed by replicating the study with loss of function approaches. As neuromodulatory mechanisms appear to be a strong candidate for mediating this phenomenon, experiments using noradrenergic and/or cholinergic antagonists could reveal whether these systems play a role in pre-stimulus modulations. Furthermore, if the source of pre-stimulus modulations can be isolated then analysis aimed at understanding how the absence of such pre-stimulus modulations shape subsequent taste processing in GC can be performed.

In the stimulus-evoked epoch, the high fidelity of spike times within the lick cycle is a very interesting phenomenon. The basis of these robust lick modulated firing rates can be investigated with loss of function experiments where regions that are hypothesized to carry this rhythmic information to GC are selectively inactivated. Given the observed lick rhythmic neurons throughout the gustatory pathway an immediate candidate region would be VPMpc. Beyond understanding the sources of these rhythmic firing rate patterns, it would be of crucial importance to study the functional importance of this rhythmic activity. In the current experimental paradigm, only the first lick provided a taste solution, it would be interesting to conduct a similar study where each lick provides a drop of solution. Such an experimental paradigm would help us understand how taste coding evolves within the envelope of rhythmic activity. This experimental design, would also allow for assessing if there is any taste specific information in spike phases.

To understand the types of information GC provides to its downstream targets, it would be interesting to label GC neurons according to their downstream targets using a combination of retrograde viral tracing and floxed ChR viral injection techniques. This would allow to record from neurons whose projections have been identified and compare the functional properties of these neurons. It would be important to understand whether GC neurons with distinct tuning curves (broad versus narrow) project to distinct regions.

Finally a very important follow-up study would be to investigate whether the observed functional properties change in a task-dependent manner. It is possible that in an experimental paradigm where animals are required to make taste based decisions (such as in go/no-go paradigms or lick-left/lick right paradigms), the cortical processing would be different. The behavioral demand of having to make taste based decisions could alter the taste coding mechanisms in GC to increase the contrast among taste representations and facilitate taste based decision making. It would be important to understand if such context dependent sensory processing exists, and if it does to understand to what extent it manifests in a layer or cell-type specific manner.

Chapter 4

4. Methods

4.1. Experimental Procedures

4.1.1. Experimental Subjects

All experimental procedures were performed according to federal, state and university regulations regarding the use of animals in research and approved by the Institutional Animal Care and Use Committee of Stony Brook University. 29 adult female mice (20-25 gr; Charles River) were subjects of this study (5 mice used in tracing and 24 mice used in electrophysiology experiments). Individually housed mice were kept in 12 hour light/ 12 hour dark cycle and were given *ad libitum* access to chow and water prior to the experimental procedures. See below for details regarding water restriction upon beginning of experiments.

4.1.2. Surgical Procedures

4.1.2.1.Chronic electrode implant surgeries

Mice were anesthetized with intraperitoneally injected ketamine/dexdomitor mixture (0.005 ml per 1gram of body weight, concentration: 13.3 mg/ml and 0.167 mg/ml respectively) and supplemented in small doses as needed (10% of initial dose). After reaching surgical levels of anesthesia, animals were put on a stereotaxic device (Narishige). Body temperature was maintained constant (36°C) throughout the surgery. The skull was exposed with a small incision, cleaned using 3% hydrogen peroxide and covered with photo-curing bone-etchant (Self Etch, Heraeus). A 1mm^2 craniotomy was performed unilaterally above gustatory cortex (stereotaxic coordinates: 1.1 mm anterior to bregma and 3.3 mm lateral to bregma). Custom-made, drivable electrode arrays, consisted of 16 wires (formvar coated 0.0015" nichrome micro-wires, A-M Systems) glued next to each other to form a linear array of 500 µm width [36]. The linear array was cut at an angle (such that electrodes spanned a 500-750 µm range along the dorsal-ventral axis) and each electrode's position within the linear array was mapped. The linear array was coated with Di (Molecular Probes) and slowly lowered until the deepest electrode reached the dorsal boundary of GC (2.5 mm ventral to bregma). We targeted our electrodes either to the superficial (3.5 mm lateral to bregma) or to the deep (2.7 mm lateral to bregma) layers of GC. The ground electrode was inserted underneath the skull, above the cerebellum. The microdrive, the ground pin and a head bolt (for head restraint) were cemented onto the skull using photo-curing dental cement (Flow-It ALC, Pentron). At the end of the surgery, animals were injected with Antisedan (0.005 ml per 1 gram of body weight, concentration 1.6 mg/ml) for reversal of anesthesia and placed on a heated pad at their home cage for recovery.

4.1.2.2.Acute recording surgical preparation

In 13 animals, we performed acute recordings targeting gustatory cortex from the lateral surface of the brain in order to sample simultaneously across layers. To prepare mice for lateral access to gustatory cortex, the ipsilateral eye was sutured closed, and the skull overlying the gustatory cortex was exposed. A recording well was built on the lateral surface using photo-curing bone etchant and photo-curing dental cement. A very thin layer of bone etchant and dental cement were also used to cover the exposed skull to prevent tissue growth in the region. After preparation of the recording well on the lateral surface, the dorsal surface of the skull was exposed and treated as described above to cement the ground wire and the head post. The animals were given 1-2 weeks to recover, before beginning the training sessions. Training lasted approximately two weeks. From 5 to 12 hours before the first experimental session, animals were anesthetized using isoflurane (2%) and a small craniotomy was performed on the lateral surface of the skull to expose the gustatory cortex. A small tear in the dura was made to facilitate the entry of the linear array. The craniotomy and duratomy were performed such that we could access the intersection between the medial cerebral artery (MCA) and the rhinal vein. This vasculature landmark has been shown to be aligned with the granular and dysgranular portions of the gustatory cortex [111]. Craniotomy was covered with Kwik-Cast and animals were returned to their home cage until the experimental session.

4.1.3. Behavioral Training and Experimental Sessions

Animals were given 1-2 weeks to recover from the surgery and water bottles were removed from the cages 48 hours prior to the first training session. In the first days of training, mice were habituated to lick sucrose solution from a moveable spout while head restrained. In the subsequent days, in addition to sucrose (0.2 M), we began delivering water, salt (0.075 M), citric acid (0.02 M) and quinine (0.001M) solutions (all dissolved in water). Once the animals habituated to head restraint and freely licked for all solutions, we switched to training the animals on the experimental trial structure where each trial began with an auditory tone (2 kHz frequency and 200 ms duration), and was followed (after 1s) by the protraction of the lick spout. The spout contained a pre-formed drop (~2 µl) of solution (one of the five stimuli), and mice had to initiate licking within 1s after the spout movement began. For a trial to be considered correct, animals had to do at least 6 licks at a minimum of 7 Hz frequency. There was no further delivery of solution after the first drop and animals had to continue licking until the sixth lick delivered a drop of water to rinse the mouth and prepare for the next trial. Spout retracted 1 second after the delivery of rinse. Trials in which animals failed to initiate licking, maintain the required lick rhythm, or do enough licks to obtain a rinse, were considered error trials and were followed by a 20 second time-out. This trial structure reinforced the natural licking pattern of mice and facilitated obtaining stereotyped licking behavior across tastants, sessions and animals. At the end of all trials, the spout was retracted and cleaned. The inter-trial interval was 3 seconds

between consecutive correct trials. Error trials and trials that were not preceded by a rinse were excluded from the analysis.

The gravity based taste delivery system consisted of five separate fluid lines that converged to a manifold at the tip of the lick spout. The system was housed inside a custom-made sound attenuating chamber. White noise was played throughout the entire session to obscure any potential auditory cues caused by opening of taste delivery valves. In addition, a fan placed by the lick spout was turned on during all sessions to obscure any potential olfactory cues from the pre-formed drop of solution. The number of skipped versus initiated trials were indistinguishable across different taste trials (data not shown), suggesting that animals did not have prior knowledge of which taste they were going to receive before contacting the taste solution. We began recording sessions once animals were doing at least hundred correct trials across all tastants, for three consecutive days. Throughout the training and experimental period, animals' water intake was limited to 1.5-2 ml/ day. Animals' weight, mobility, grooming behavior and posture were monitored daily to ensure mice were healthy, and additional water was offered if animals showed signs of dehydration.

4.1.4. Electrophysiological Recordings

Extracellularly recorded signals were amplified, band-pass filtered (300-8000 Hz), digitized and recorded (at 40 KHz) using a Plexon MAP system. Single units were isolated using Offline Sorter software (Plexon). Clustering of waveform features in principal component space as well as analysis of inter-spike interval histograms were used to isolate action potentials recorded from a single unit [22, 23, 87, 97]. Data were analyzed using custom-written software in Matlab (MathWorks, Inc.).

4.1.4.1.Chronic Recordings

Linear arrays of electrodes, implanted chronically from the dorsal surface of the skull, were lowered 100 μm at the end of each experimental session. This allowed us to obtain recordings from a new subset of neurons in the subsequent recording session from the same animal. The electrodes were lowered until the most dorsal wire reached the ventral boundary of gustatory cortex as determined by stereotaxic coordinates. Only recordings from the gustatory cortex, as verified by recording depth and post-hoc histological sections were included in the analysis.

4.1.4.2.Acute Recordings

Mice were head restrained; Kwik-Cast covering the craniotomy was removed and replaced with cortex buffer to protect the surface of the craniotomy. A 16 channel linear array, coated with Di (Molecular Probes), was targeted to the gustatory cortex using the intersection between the medial cerebral artery and the rhinal veins as a landmark (see *Acute recording surgical preparation*). The array was inserted orthogonal to the cortical surface and guided using a micromanipulator (Narishige) at approximately 200 µm/min speed. After the final position was reached (deepest wire at 1000 µm), the craniotomy was covered with 30.000 cs Dow-Corning silicon (Advance Weight Systems Inc.) to stabilize the linear array. To further ensure stability of recordings, we waited 30 mins before beginning the experimental session. Mice in acute recording group had been previously habituated to sit comfortably in head restraint for extended periods of time to facilitate this idle period before the experimental session began. At the end of each experimental session, the linear array was retracted, the silicone was removed and the craniotomy was covered with Kwik-Cast before returning the animal to its home cage. We limited our acute recordings to two sessions per animal in order to minimize tissue damage within the recording site.

4.1.5. Retrograde Tracer Injections

In five mice, 100 nl of cholera-toxin subunit B conjugated to Alexa Fluor 555 (CTB 555), (Molecular Probes) was injected unilaterally into gustatory cortex (stereotaxic coordinates from bregma; AP: +1 mm, ML: 3.94 mm, DV: -2.4 mm). A sharp glass pipette was pulled (Sutter Instruments) the tip was broken, filled with mineral oil and back filled with 500 nl of CTB 555. The glass pipette was inserted into Nanoject (Drummond Scientific), and slowly lowered into gustatory cortex using a micromanipulator (Narishige). 20 puffs of ~5nl solution were delivered into the region. We waited one minute between each puff to allow the toxin to spread away from the pipette tip. After the final puff, we waited 15 minutes to minimize the spread of the toxin to more dorsal areas before slowly retracting the pipette. The skin was sutured closed and the animals were returned to their home cage to recover. Animals were sacrificed 2 weeks after the surgery. The brains were processed as described below.

4.1.6. Histological Procedures

At the end of experiments, mice were administered a lethal dose of ketamine/dexdomitor mixture and transcardially perfused using phosphate-buffered saline (PBS) followed by 4% paraformaldehyde (PFA) dissolved in PBS. Brains were removed and post-fixed in 4% PFA overnight. 50-100 µm thick coronal sections were cut using a Leica vibratome. Brain slices were mounted with media containing fluorescent DAPI to visualize cell nuclei (Fluoromount, Electron Microscopy Sciences). Standard confocal microcopy procedures (Olympus) were used to image the coronal sections and identify the anatomical location of the electrode track as marked by Di

stain. For tracing experiments, the retrogradely filled cell bodies were visualized and imaged using 20X magnification.

4.2. Data Analysis

4.2.1. Layer assignments

Neurons were classified as belonging to deep (infragranular) layers or superficial (supragranular) layers based on the recording site and post-hoc histological sections. In chronic recording configuration, we used the channel mapping, the histology sections and the recording depth (along the dorsal-ventral axis) to triangulate the position of each electrode wire in a given session. In animals where all the wires of the linear array were positioned deeper than layer 4 (as shown in Fig 7D) the recordings were classified as deep layer recordings. In animals where all the wires of the linear arrays were targeted more superficial than layer 4 (as shown in Fig 7E) were classified as superficial recordings. Single units isolated from electrodes with ambiguous layer assignments were excluded from analysis. In acute recordings, where electrodes were inserted orthogonally to the cortical surface, we used micro-manipulator read-out, combined with the channel mapping to determine the depth of each channel. Single units recorded deeper than 420 μm were classified as deep layer neurons and single units recorded between 0-420 μm were classified as superficial layer neurons.

4.2.2. Cell type assignments

Isolated single units were classified as putative excitatory or putative inhibitory neurons based on the width of the extracellularly recorded waveforms as described previously in the literature [50, 58]. The width of the waveform was measured as the interval from the trough to the peak (in μs). MATLAB's built in k-means clustering algorithm was used to classify neurons into two distinct categories based on the width of the waveforms. Histogram of spike width values of the resulting clusters revealed two non-overlapping distributions.

4.2.3. Area under the curve normalization

For visualization and analysis of population activity, firing rates of single neurons were normalized using the non-parametric area under the receiver operating curve (auROC) method [22, 87, 127]. The specifics on how to implement this method can be found in [127]. Briefly, stimulus evoked firing rate of each neuron is normalized to range between 0-1, where 0.5 represents the baseline firing rate. Excitatory deviations from baseline activity are valued as > 0.5 and inhibitory deviations from baseline activity are valued as < 0.5.

4.2.4. Mouth Movement Analysis

Orofacial behavior was recorded for 42/80 experimental sessions (124/223 units) (at 30 frames/second rate). Video, neural recording, and event time-stamps were synchronized using Cineplex software (Plexon). Videos from experimental sessions were imported (AVI format) and analyzed using custom-written software in MATLAB [21, 22]. The orofacial region was cropped (as shown in Fig. 11A, left panel, excluding the whiskers and the nose) and mouth movement analysis was performed on this selected region. For each trial, the mouth movement signal was extracted as the absolute difference in pixel intensity between consecutive frames. For each session, the mouth movement signal was normalized to range between 0-100 where the maximum change in pixel intensity, which occurred when the animal was licking the spout, was set to equal 100, and the signal with no mouth movement was set to equal to 0. For 124 neurons recorded in 42 sessions, cross-correlations between mouth movement and spiking activity (using 33ms bin size to match mouth movement sampling rate) were computed on mean subtracted signals during the 3 second inter-trial interval (3s interval prior to the auditory tone onset) on a trial by trial basis. Cross correlations were then averaged across trials and the area under the resulting cross correlation curve (auXCC) was computed. The significance of cross-correlations was assessed by comparing the auXCC of session average to a null distribution of auXCC .The null auXCC distribution was created by shuffling the trials of the session. The auXCC value for the trial-shuffled session was computed in the same way as described above for the experimental session. We repeated this step 1000 times to obtain the null auXCC distribution and the significance of the experimentally obtained auXCC was tested at alpha=0.05. For neurons with significant cross correlations, we determined which signal was the preceding signal (mouth movement or firing rate) by comparing the area under the curve to the left versus the right of the lag=0 point. The significance of $((Left\ auXCC) - (Right\ auXCC))$ value was assessed by comparing it to the null distribution of the same parameter obtained by shuffling trials as described above. This analysis yielded three categories of neurons; neurons with significant cross-correlations but no discernable lag (broad), neurons with significant cross-correlations with mouth movement preceding spikes (MM precedes), neurons with significant cross-correlations with spikes preceding mouth movement (FR precedes). Using the area under the curve method bypasses the multiple comparisons issue that arises when testing the significance of cross correlations against the null distribution at each lag point.

4.2.5. Pre-Stimulus Modulation Analysis

For each neuron, trials were aligned to the onset of the first lick. The 500 ms interval prior to the first lick was divided into two 250 ms bins. Distribution of firing rates obtained from each pre-stimulus bin was compared to firing rates obtained from baseline (1 second baseline, taken as the 1 second prior to the onset of the auditory cue, divided into four 250 ms bins and concatenated across trials) using a two-sided, unbalanced Mann-Whitney U test at $p < 0.05$. Familywise error rate introduced by comparing two bins to baseline was controlled using Dunn-Sidak correction. Neurons with significantly greater firing rates than baseline in at least one pre-

stimulus bin were classified as pre-stimulus excited, and neurons with significantly lower firing rates than baseline in at least one pre-stimulus bin were classified as pre-stimulus inhibited. Repeating the analysis with different bin sizes yielded similar results. To assess whether pre-stimulus modulations were driven by spout movement or lick-related movement, we generated two PSTHs for each pre-stimulus excited neuron: one PSTH aligned to the onset of the spout-movement and one PSTH aligned to the onset of the first-lick (as shown in Fig. 10A and 10B respectively). For each PSTH, we only included spikes that occurred in the interval between the spout onset and the first lick. This ensured that we included the same spike count in each trial for both PSTH types and the only differences we observed were due to the differences in alignment rather than spike count. We then computed the maximum firing rate of each PSTH and visualized the spout-onset aligned versus first-lick aligned maximum firing rates on a scatter plot. All pre-stimulus excitatory modulated neurons had higher maximum firing rate when the activity was aligned to the first-lick as opposed to the spout onset. In a second analysis on pre-stimulus excited neurons, we quantified the distance of each spike that occurred within the spout offset to lick onset interval either to the lick onset or to the spout offset. Distributions of spike distances to either event were compared using. We limited our analysis to pre-stimulus excited neurons as increases in firing rate were more robust than decreases in firing rates. We argue that the driving cause of the pre-stimulus modulations are very unlikely to be different for pre-stimulus excited versus pre-stimulus inhibited neurons and therefor reason that findings from pre-stimulus excited neurons showing that their modulation is aligned to the first-lick onset can also be extended to pre-stimulus inhibited neurons.

4.2.6. Change point analysis

To assess the onset of modulation, pre-stimulus modulated neurons were analyzed. All trials were aligned to the first-lick, and the 500 ms interval prior to the lick onset was tested for a significant change point. The first change point in this 500 ms interval was deemed the onset of pre-stimulus modulation. The details of this method can be found in [97, 128]. Briefly, the change point method computes the cumulative distribution function of spike occurrences over the baseline (1 second baseline prior to auditory cue) and pre-stimulus epoch. The time point in which the slope of the CDF in the pre-stimulus epoch exceeds the slope distribution obtained from the baseline epoch, is marked as a change point.

4.2.7. Stimulus-Evoked Modulation Analysis

Trials were aligned to the onset of the first lick and the first 500 ms following the lick onset were divided into two 250 ms bins. We limited our analysis to the first 500 ms window after the first-lick onset as the rinse delivery occurred in the 500-600 ms interval. Only trials that satisfied the behavioral criteria as described above (see *Experimental Sessions*) were analyzed. Stimulus-evoked firing rates were compared to baseline firing rates (1 second baseline prior to

the auditory cue, divided into four 250 ms bins and all bins concatenated across trials) using two-sided, unbalanced Mann-Whitney U test at $p < 0.05$. Neurons with significantly greater stimulus-evoked firing rates than baseline were classified as stimulus excited and neurons with significantly smaller stimulus-evoked firing rates than baseline were classified as stimulus inhibited.

4.2.8. Rhythmic Modulation of Firing Rate in Stimulus Evoked Epoch

For each neuron, only the trials where mice maintained 7 Hz licking rhythm for at least seven consecutive licks were used for this analysis. For each spike that occurred within the first 7 lick cycles, the relative position of the spike with respect to its corresponding lick cycle was computed in radians. The details of this lick-warping method are described below in *Spike Phase Consistency* section. The power spectrum density was computed for the lick warped PSTHs using Matlab's built in *periodogram* script using 2-20 Hz band-pass filter and $\boldsymbol{\pi}/60$ radian bin size (corresponds to ~1.1 ms). Power spectra were normalized so that the sum of the signal was 100. A neuron's firing rate pattern was classified as rhythmically modulated if the neuron's power spectrum had a peak in the 6-10 Hz range, and if the amplitude of the peak was at least 2 standard deviations greater than the median value of the signal.

4.2.9. Spike Phase Consistency

For each neuron, only the trials where mice maintained 7 Hz licking rhythm for at least seven consecutive licks were used for this analysis. For each spike that occurred within the first 7 lick cycles, the relative position of the spike with respect to its corresponding lick cycle was computed in radians using the following formula:

$$(2 * \pi) * \left(\frac{Spike\ Time - Lick\ Begin}{Lick\ Cycle}\right)$$

The variables *Spike time*, *Lick begin* and *Lick cycle* were computed in seconds. *Lick cycle* was computed as the duration between two consecutive licks. Since each lick cycle is slightly different in duration (inter-lick interval mean= 0.135 seconds, std= 0. 035 seconds) converting spike times from seconds to radians allowed us to quantify the relative position of the spike with respect to the lick cycle and compare across trials, sessions and animals.

After all the spike times were converted to radians ranging from $0\boldsymbol{\pi}$ -$2\boldsymbol{\pi}$ radians, the $0\boldsymbol{\pi}$ -$2\boldsymbol{\pi}$ interval was then divided into 8 bins. We call each of these bins a *phase-bin*. On average $2\boldsymbol{\pi}$

radians corresponded to 135 ms, therefore each phase-bin was roughly equivalent to 17 ms. We computed the probability of observing a spike in a particular phase-bin given the neuron's total spike count for all the phase-bins. We then compared this probability distribution to a uniform probability distribution (i.e the case in which the probability of observing a spike is the same across all phase-bins of the lick cycle). The uniform probability distribution was given by (*1/ number of Bins*). The difference between the observed and the uniform probability distribution was quantified using *total variation distance* and standardized by dividing by the number of trials. Using this measure, neurons that spike reliably during a specific phase of the lick cycle yield large total variation values, whereas neurons that spike uniformly throughout the lick cycle have small total variation values. Spike phase consistency measure across cell categories was compared using Kruskal-Wallis test followed by multiple comparisons using Bonferroni correction. Varying the bin size did not alter the results across four different bin sizes we tested.

We opted to use the Spike Phase Consistency measure to assess whether spikes occur preferentially at specific phases of the lick cycle instead of the R-value (mean vector length of the circular spike phase distribution). This is because the R-value does not capture the consistency of spike phase when spike phases are distributed in a bimodal or multimodal manner (see rose plot of representative neuron SI in Figure 13A).

4.2.10. Spike Count Consistency

To assess the consistency in the number of spikes evoked by each lick across trials, we created a spike count matrix (*Trials * Lick cycles*) from the lick warped data of each neuron. The probability distribution of observing a spike in a given lick cycle of a single trial, was compared to the uniform probability distribution (i.e where each lick cycle of each trial had the same probability of emitting a spike). The distance between the observed probability distribution and the uniform probability distribution was computed using the total variation measure as described above. The total variation value was standardized by dividing it by *Number of trials* in order to prevent biasing the measure with the variation in number of trials. The final value was subtracted from 1 so that neurons with very small deviation from a uniform probability distribution would have a value close to 1 and neurons with large deviation would have a value closer to 0. Using this measure, $\left(1 - \left(\frac{Total\ Variation}{Number\ of\ Trials}\right)\right)$, neurons whose firing rate varied little from trial to trial and lick to lick had larger spike count consistency values compared to neurons whose firing rate was highly variable from trial to trial and lick to lick.

4.2.11. Taste Coding Analysis

Two-way ANOVA (*Tastants*Lick Bin*) was used to assess whether a neuron had different response profiles across tastants. We used lick-warped data for this analysis and only included the first five lick bins to capture exclusively the activity that occurred prior to the rinse. The duration of each lick bin is approximately 135 ms. For a given neuron, trial counts of all tastants were matched to that with the lowest trial count by randomly selecting a subset of trials. A neuron was classified as taste-coding (i.e. chemosensitive) if the p-value of the taste term or the p-value of *Taste*Lick Bin* interaction term was smaller than 0.05. If a neuron was chemosensitive, we further analyzed how many tastants the neuron was able to differentiate from water by doing a post-hoc multiple comparisons test. The neuron was said to be differentiating between the given tastant and water if the response to the tastant was significantly different than that of water after a Bonferroni correction.

Bibliography

1. Harris, K.D. and T.D. Mrsic-Flogel, *Cortical connectivity and sensory coding.* Nature, 2013. **503**(7474): p. 51-8.
2. Harris, K.D. and G.M. Shepherd, *The neocortical circuit: themes and variations.* Nat Neurosci, 2015. **18**(2): p. 170-81.
3. Shepherd, G.M., *The microcircuit concept applied to cortical evolution: from three-layer to six-layer cortex.* Front Neuroanat, 2011. **5**: p. 30.
4. Poo, C. and J.S. Isaacson, *Odor representations in olfactory cortex: "sparse" coding, global inhibition, and oscillations.* Neuron, 2009. **62**(6): p. 850-61.
5. Franks, K.M. and J.S. Isaacson, *Strong single-fiber sensory inputs to olfactory cortex: implications for olfactory coding.* Neuron, 2006. **49**(3): p. 357-63.
6. Niell, C.M. and M.P. Stryker, *Highly selective receptive fields in mouse visual cortex.* J Neurosci, 2008. **28**(30): p. 7520-36.
7. Otazu, G.H., et al., *Engaging in an auditory task suppresses responses in auditory cortex.* Nat Neurosci, 2009. **12**(5): p. 646-54.
8. Wehr, M. and A.M. Zador, *Balanced inhibition underlies tuning and sharpens spike timing in auditory cortex.* Nature, 2003. **426**(6965): p. 442-6.
9. Petersen, C., *Cell-type specific function of GABAergic neurons in layers 2 and 3 of mouse barrel cortex.* Curr Opin Neurobiol, 2014. **26**: p. 1-6.
10. Petersen, C.C. and S. Crochet, *Synaptic computation and sensory processing in neocortical layer 2/3.* Neuron, 2013. **78**(1): p. 28-48.
11. Gentet, L.J., et al., *Unique functional properties of somatostatin-expressing GABAergic neurons in mouse barrel cortex.* Nat Neurosci, 2012. **15**(4): p. 607-12.
12. Mateo, C., et al., *In vivo optogenetic stimulation of neocortical excitatory neurons drives brain-state-dependent inhibition.* Curr Biol, 2011. **21**(19): p. 1593-602.
13. Crochet, S., et al., *Synaptic mechanisms underlying sparse coding of active touch.* Neuron, 2011. **69**(6): p. 1160-75.
14. Crochet, S. and C.C. Petersen, *Cortical dynamics by layers.* Neuron, 2009. **64**(3): p. 298-300.
15. Crochet, S. and C.C. Petersen, *Correlating whisker behavior with membrane potential in barrel cortex of awake mice.* Nat Neurosci, 2006. **9**(5): p. 608-10.
16. Petersen, C.C., et al., *Interaction of sensory responses with spontaneous depolarization in layer 2/3 barrel cortex.* Proc Natl Acad Sci U S A, 2003. **100**(23): p. 13638-43.
17. O'Connor, D.H., et al., *Neural activity in barrel cortex underlying vibrissa-based object localization in mice.* Neuron, 2010. **67**(6): p. 1048-61.
18. Katz, D.B., S.A. Simon, and M.A. Nicolelis, *Taste-specific neuronal ensembles in the gustatory cortex of awake rats.* J Neurosci, 2002. **22**(5): p. 1850-7.
19. Samuelsen, C.L. and A. Fontanini, *Processing of Intraoral Olfactory and Gustatory Signals in the Gustatory Cortex of Awake Rats.* J Neurosci, 2017. **37**(2): p. 244-257.
20. Gutierrez, R., S.A. Simon, and M.A. Nicolelis, *Licking-induced synchrony in the taste-reward circuit improves cue discrimination during learning.* J Neurosci, 2010. **30**(1): p. 287-303.
21. Vincis, R. and A. Fontanini, *Associative learning changes cross-modal representations in the gustatory cortex.* Elife, 2016. **5**.
22. Gardner, M.P. and A. Fontanini, *Encoding and tracking of outcome-specific expectancy in the gustatory cortex of alert rats.* J Neurosci, 2014. **34**(39): p. 13000-17.

23. Samuelsen, C.L., M.P. Gardner, and A. Fontanini, *Effects of cue-triggered expectation on cortical processing of taste.* Neuron, 2012. **74**(2): p. 410-22.
24. Grossman, S.E., et al., *Learning-related plasticity of temporal coding in simultaneously recorded amygdala-cortical ensembles.* J Neurosci, 2008. **28**(11): p. 2864-73.
25. Accolla, R. and A. Carleton, *Internal body state influences topographical plasticity of sensory representations in the rat gustatory cortex.* Proc Natl Acad Sci U S A, 2008. **105**(10): p. 4010-5.
26. Constantinople, C.M. and R.M. Bruno, *Deep cortical layers are activated directly by thalamus.* Science, 2013. **340**(6140): p. 1591-4.
27. Smith, P.H., et al., *Thalamocortical projections to rat auditory cortex from the ventral and dorsal divisions of the medial geniculate nucleus.* J Comp Neurol, 2012. **520**(1): p. 34-51.
28. Thomson, A.M. and C. Lamy, *Functional maps of neocortical local circuitry.* Front Neurosci, 2007. **1**(1): p. 19-42.
29. Mease, R.A., P. Krieger, and A. Groh, *Cortical control of adaptation and sensory relay mode in the thalamus.* Proc Natl Acad Sci U S A, 2014. **111**(18): p. 6798-803.
30. Velez-Fort, M., et al., *The stimulus selectivity and connectivity of layer six principal cells reveals cortical microcircuits underlying visual processing.* Neuron, 2014. **83**(6): p. 1431-43.
31. Matyas, F., et al., *Motor control by sensory cortex.* Science, 2010. **330**(6008): p. 1240-3.
32. Hooks, B.M., et al., *Organization of cortical and thalamic input to pyramidal neurons in mouse motor cortex.* J Neurosci, 2013. **33**(2): p. 748-60.
33. Kepecs, A. and G. Fishell, *Interneuron cell types are fit to function.* Nature, 2014. **505**(7483): p. 318-26.
34. Rudy, B., et al., *Three groups of interneurons account for nearly 100% of neocortical GABAergic neurons.* Dev Neurobiol, 2011. **71**(1): p. 45-61.
35. DeFelipe, J., et al., *New insights into the classification and nomenclature of cortical GABAergic interneurons.* Nat Rev Neurosci, 2013. **14**(3): p. 202-16.
36. Krupa, D.J., et al., *Layer-specific somatosensory cortical activation during active tactile discrimination.* Science, 2004. **304**(5679): p. 1989-92.
37. de Kock, C.P., et al., *Layer- and cell-type-specific suprathreshold stimulus representation in rat primary somatosensory cortex.* J Physiol, 2007. **581**(Pt 1): p. 139-54.
38. Barth, A.L. and J.F. Poulet, *Experimental evidence for sparse firing in the neocortex.* Trends Neurosci, 2012. **35**(6): p. 345-55.
39. Sakata, S. and K.D. Harris, *Laminar-dependent effects of cortical state on auditory cortical spontaneous activity.* Front Neural Circuits, 2012. **6**: p. 109.
40. Isaacson, J.S. and M. Scanziani, *How Inhibition Shapes Cortical Activity.* Neuron, 2011. **72**(2): p. 231-243.
41. Kerlin, A.M., et al., *Broadly Tuned Response Properties of Diverse Inhibitory Neuron Subtypes in Mouse Visual Cortex.* Neuron, 2010. **67**(5): p. 858-871.
42. Liu, B.H., et al., *Visual Receptive Field Structure of Cortical Inhibitory Neurons Revealed by Two-Photon Imaging Guided Recording.* Journal of Neuroscience, 2009. **29**(34): p. 10520-10532.
43. Liu, B.H., et al., *Broad Inhibition Sharpens Orientation Selectivity by Expanding Input Dynamic Range in Mouse Simple Cells.* Neuron, 2011. **71**(3): p. 542-554.

44. Sohya, K., et al., *GABAergic neurons are less selective to stimulus orientation than excitatory neurons in layer II/III of visual cortex, as revealed by in vivo functional Ca2+ imaging in transgenic mice.* Journal of Neuroscience, 2007. **27**(8): p. 2145-2149.
45. Poo, C. and J.S. Isaacson, *Odor Representations in Olfactory Cortex: "Sparse" Coding, Global Inhibition, and Oscillations.* Neuron, 2009. **62**(6): p. 850-861.
46. Bock, D.D., et al., *Network anatomy and in vivo physiology of visual cortical neurons.* Nature, 2011. **471**(7337): p. 177-U59.
47. Fino, E. and R. Yuste, *Dense inhibitory connectivity in neocortex.* Neuron, 2011. **69**(6): p. 1188-203.
48. Packer, A.M. and R. Yuste, *Dense, unspecific connectivity of neocortical parvalbumin-positive interneurons: a canonical microcircuit for inhibition?* J Neurosci, 2011. **31**(37): p. 13260-71.
49. Ko, H., et al., *Functional specificity of local synaptic connections in neocortical networks.* Nature, 2011. **473**(7345): p. 87-91.
50. Cardin, J.A., L.A. Palmer, and D. Contreras, *Stimulus feature selectivity in excitatory and inhibitory neurons in primary visual cortex.* Journal of Neuroscience, 2007. **27**(39): p. 10333-10344.
51. Liu, B.H., et al., *Intervening inhibition underlies simple-cell receptive field structure in visual cortex.* Nat Neurosci, 2010. **13**(1): p. 89-96.
52. Wilent, W.B. and D. Contreras, *Dynamics of excitation and inhibition underlying stimulus selectivity in rat somatosensory cortex.* Nat Neurosci, 2005. **8**(10): p. 1364-70.
53. Wang, J., D. Caspary, and R.J. Salvi, *GABA-A antagonist causes dramatic expansion of tuning in primary auditory cortex.* Neuroreport, 2000. **11**(5): p. 1137-40.
54. Katzner, S., L. Busse, and M. Carandini, *GABAA inhibition controls response gain in visual cortex.* J Neurosci, 2011. **31**(16): p. 5931-41.
55. Kyriazi, H.T., et al., *Quantitative effects of GABA and bicuculline methiodide on receptive field properties of neurons in real and simulated whisker barrels.* J Neurophysiol, 1996. **75**(2): p. 547-60.
56. Tan, A.Y., et al., *Tone-evoked excitatory and inhibitory synaptic conductances of primary auditory cortex neurons.* J Neurophysiol, 2004. **92**(1): p. 630-43.
57. Sakata, S. and K.D. Harris, *Laminar structure of spontaneous and sensory-evoked population activity in auditory cortex.* Neuron, 2009. **64**(3): p. 404-18.
58. Niell, C.M. and M.P. Stryker, *Highly selective receptive fields in mouse visual cortex.* Journal of Neuroscience, 2008. **28**(30): p. 7520-7536.
59. Iurilli, G., et al., *Sound-driven synaptic inhibition in primary visual cortex.* Neuron, 2012. **73**(4): p. 814-28.
60. Brosch, M., E. Selezneva, and H. Scheich, *Nonauditory events of a behavioral procedure activate auditory cortex of highly trained monkeys.* J Neurosci, 2005. **25**(29): p. 6797-806.
61. Lakatos, P., et al., *Neuronal oscillations and multisensory interaction in primary auditory cortex.* Neuron, 2007. **53**(2): p. 279-92.
62. Maier, J.X., *Single-neuron responses to intraoral delivery of odor solutions in primary olfactory and gustatory cortex.* J Neurophysiol, 2017. **117**(3): p. 1293-1304.
63. Maier, J.X., M. Wachowiak, and D.B. Katz, *Chemosensory convergence on primary olfactory cortex.* J Neurosci, 2012. **32**(48): p. 17037-47.

64. Vinck, M., et al., *Arousal and locomotion make distinct contributions to cortical activity patterns and visual encoding.* Neuron, 2015. **86**(3): p. 740-54.
65. Fontanini, A. and D.B. Katz, *State-dependent modulation of time-varying gustatory responses.* J Neurophysiol, 2006. **96**(6): p. 3183-93.
66. Fontanini, A. and D.B. Katz, *7 to 12 Hz activity in rat gustatory cortex reflects disengagement from a fluid self-administration task.* J Neurophysiol, 2005. **93**(5): p. 2832-40.
67. Eggermann, E., et al., *Cholinergic signals in mouse barrel cortex during active whisker sensing.* Cell Rep, 2014. **9**(5): p. 1654-60.
68. Poulet, J.F., et al., *Thalamic control of cortical states.* Nat Neurosci, 2012. **15**(3): p. 370-2.
69. Samuelsen, C.L., M.P. Gardner, and A. Fontanini, *Thalamic contribution to cortical processing of taste and expectation.* J Neurosci, 2013. **33**(5): p. 1815-27.
70. Reimer, J., et al., *Pupil fluctuations track rapid changes in adrenergic and cholinergic activity in cortex.* Nat Commun, 2016. **7**: p. 13289.
71. Reimer, J., et al., *Pupil fluctuations track fast switching of cortical states during quiet wakefulness.* Neuron, 2014. **84**(2): p. 355-62.
72. Poulet, J.F. and C.C. Petersen, *Internal brain state regulates membrane potential synchrony in barrel cortex of behaving mice.* Nature, 2008. **454**(7206): p. 881-5.
73. Fontanini, A. and D.B. Katz, *Behavioral states, network states, and sensory response variability.* J Neurophysiol, 2008. **100**(3): p. 1160-8.
74. Niell, C.M. and M.P. Stryker, *Modulation of visual responses by behavioral state in mouse visual cortex.* Neuron, 2010. **65**(4): p. 472-9.
75. Zhou, M., et al., *Scaling down of balanced excitation and inhibition by active behavioral states in auditory cortex.* Nature Neuroscience, 2014. **17**(6): p. 841-850.
76. Qi, R., et al., *State-dependent changes in auditory sensory gating in different cortical areas in rats.* PLoS One, 2015. **10**(4): p. e0126684.
77. Murakami, M., et al., *State-dependent sensory gating in olfactory cortex.* Neuron, 2005. **46**(2): p. 285-96.
78. Liman, E.R., Y.V. Zhang, and C. Montell, *Peripheral coding of taste.* Neuron, 2014. **81**(5): p. 984-1000.
79. Carleton, A., R. Accolla, and S.A. Simon, *Coding in the mammalian gustatory system.* Trends Neurosci, 2010. **33**(7): p. 326-34.
80. Di Lorenzo, P.M. and S. Monroe, *Corticofugal influence on taste responses in the nucleus of the solitary tract in the rat.* J Neurophysiol, 1995. **74**(1): p. 258-72.
81. Monroe, S. and P.M. Di Lorenzo, *Taste responses in neurons in the nucleus of the solitary tract that do and do not project to the parabrachial pons.* J Neurophysiol, 1995. **74**(1): p. 249-57.
82. Roussin, A.T., et al., *Taste coding in the nucleus of the solitary tract of the awake, freely licking rat.* J Neurosci, 2012. **32**(31): p. 10494-506.
83. Hayama, T., S. Ito, and H. Ogawa, *Responses of solitary tract nucleus neurons to taste and mechanical stimulations of the oral cavity in decerebrate rats.* Exp Brain Res, 1985. **60**(2): p. 235-42.
84. Travers, S.P. and R. Norgren, *Organization of orosensory responses in the nucleus of the solitary tract of rat.* J Neurophysiol, 1995. **73**(6): p. 2144-62.

85. Weiss, M.S., J.D. Victor, and P.M. Di Lorenzo, *Taste coding in the parabrachial nucleus of the pons in awake, freely licking rats and comparison with the nucleus of the solitary tract.* J Neurophysiol, 2014. **111**(8): p. 1655-70.
86. Di Lorenzo, P.M., *Taste responses in the parabrachial pons of decerebrate rats.* J Neurophysiol, 1988. **59**(6): p. 1871-87.
87. Liu, H. and A. Fontanini, *State Dependency of Chemosensory Coding in the Gustatory Thalamus (VPMpc) of Alert Rats.* J Neurosci, 2015. **35**(47): p. 15479-91.
88. Verhagen, J.V., B.K. Giza, and T.R. Scott, *Responses to taste stimulation in the ventroposteromedial nucleus of the thalamus in rats.* J Neurophysiol, 2003. **89**(1): p. 265-75.
89. Nomura, T. and H. Ogawa, *The taste and mechanical response properties of neurons in the parvicellular part of the thalamic posteromedial ventral nucleus of the rat.* Neurosci Res, 1985. **3**(2): p. 91-105.
90. Allen, G.V., et al., *Organization of visceral and limbic connections in the insular cortex of the rat.* J Comp Neurol, 1991. **311**(1): p. 1-16.
91. Turner, B.H. and M. Herkenham, *Thalamoamygdaloid projections in the rat: a test of the amygdala's role in sensory processing.* J Comp Neurol, 1991. **313**(2): p. 295-325.
92. Haley, M.S., A. Fontanini, and A. Maffei, *Laminar- and Target-Specific Amygdalar Inputs in Rat Primary Gustatory Cortex.* J Neurosci, 2016. **36**(9): p. 2623-37.
93. McDonald, A.J., *Cortical pathways to the mammalian amygdala.* Prog Neurobiol, 1998. **55**(3): p. 257-332.
94. Sadacca, B.F., J.T. Rothwax, and D.B. Katz, *Sodium concentration coding gives way to evaluative coding in cortex and amygdala.* J Neurosci, 2012. **32**(29): p. 9999-10011.
95. Fontanini, A., et al., *Distinct subtypes of basolateral amygdala taste neurons reflect palatability and reward.* J Neurosci, 2009. **29**(8): p. 2486-95.
96. Rolls, E.T., *Taste, olfactory, and food reward value processing in the brain.* Prog Neurobiol, 2015. **127-128**: p. 64-90.
97. Jezzini, A., et al., *Processing of hedonic and chemosensory features of taste in medial prefrontal and insular networks.* J Neurosci, 2013. **33**(48): p. 18966-78.
98. Niu, J.G., et al., *Glutamatergic lateral parabrachial neurons innervate orexin-containing hypothalamic neurons in the rat.* Brain Res, 2010. **1358**: p. 110-22.
99. Tokita, K., T. Inoue, and J.D. Boughter, Jr., *Subnuclear organization of parabrachial efferents to the thalamus, amygdala and lateral hypothalamus in C57BL/6J mice: a quantitative retrograde double labeling study.* Neuroscience, 2010. **171**(1): p. 351-65.
100. Wu, Q. and R.D. Palmiter, *GABAergic signaling by AgRP neurons prevents anorexia via a melanocortin-independent mechanism.* Eur J Pharmacol, 2011. **660**(1): p. 21-7.
101. Maffei, A., M. Haley, and A. Fontanini, *Neural processing of gustatory information in insular circuits.* Curr Opin Neurobiol, 2012. **22**(4): p. 709-16.
102. Adachi, K., et al., *Anatomical and electrophysiological mechanisms for asymmetrical excitatory propagation in the rat insular cortex: in vivo optical imaging and whole-cell patch-clamp studies.* J Comp Neurol, 2013. **521**(7): p. 1598-613.
103. Fujita, S., et al., *Spatiotemporal profiles of transcallosal connections in rat insular cortex revealed by in vivo optical imaging.* Neuroscience, 2012. **206**: p. 201-11.
104. Holtz, S.L., et al., *Morphology and connectivity of parabrachial and cortical inputs to gustatory thalamus in rats.* J Comp Neurol, 2015. **523**(1): p. 139-61.

105. Hayama, T., K. Hashimoto, and H. Ogawa, *Anatomical location of a taste-related region in the thalamic reticular nucleus in rats.* Neurosci Res, 1994. **18**(4): p. 291-9.
106. Gabbott, P.L., et al., *Areal and synaptic interconnectivity of prelimbic (area 32), infralimbic (area 25) and insular cortices in the rat.* Brain Res, 2003. **993**(1-2): p. 59-71.
107. Wright, C.I. and H.J. Groenewegen, *Patterns of overlap and segregation between insular cortical, intermediodorsal thalamic and basal amygdaloid afferents in the nucleus accumbens of the rat.* Neuroscience, 1996. **73**(2): p. 359-73.
108. Fu, W., et al., *Convergence of olfactory and gustatory connections onto the endopiriform nucleus in the rat.* Neuroscience, 2004. **126**(4): p. 1033-41.
109. Kobayashi, M., et al., *Functional mapping of gustatory neurons in the insular cortex revealed by pERK-immunohistochemistry and in vivo optical imaging.* Synapse, 2010. **64**(4): p. 323-34.
110. Accolla, R., et al., *Differential spatial representation of taste modalities in the rat gustatory cortex.* J Neurosci, 2007. **27**(6): p. 1396-404.
111. Chen, X., et al., *A gustotopic map of taste qualities in the mammalian brain.* Science, 2011. **333**(6047): p. 1262-6.
112. Ogawa, H., K. Hasegawa, and N. Murayama, *Difference in taste quality coding between two cortical taste areas, granular and dysgranular insular areas, in rats.* Exp Brain Res, 1992. **91**(3): p. 415-24.
113. Ogawa, H., N. Murayama, and K. Hasegawa, *Difference in receptive field features of taste neurons in rat granular and dysgranular insular cortices.* Exp Brain Res, 1992. **91**(3): p. 408-14.
114. Kosar, E., H.J. Grill, and R. Norgren, *Gustatory cortex in the rat. I. Physiological properties and cytoarchitecture.* Brain Res, 1986. **379**(2): p. 329-41.
115. Ogawa, H., et al., *Taste area in granular and dysgranular insular cortices in the rat identified by stimulation of the entire oral cavity.* Neurosci Res, 1990. **9**(3): p. 196-201.
116. Katz, D.B., S.A. Simon, and M.A. Nicolelis, *Dynamic and multimodal responses of gustatory cortical neurons in awake rats.* J Neurosci, 2001. **21**(12): p. 4478-89.
117. Stapleton, J.R., et al., *Rapid taste responses in the gustatory cortex during licking.* J Neurosci, 2006. **26**(15): p. 4126-38.
118. Stapleton, J.R., et al., *Ensembles of gustatory cortical neurons anticipate and discriminate between tastants in a single lick.* Front Neurosci, 2007. **1**(1): p. 161-74.
119. Yokota, T., K. Eguchi, and T. Satoh, *Differential taste coding of salt and acid by correlative activities between taste-sensitive neuron types in rat gustatory cortex.* Neuroscience, 2007. **144**(1): p. 314-24.
120. Yokota, T., K. Eguchi, and K. Hiraba, *Functional properties of putative pyramidal neurons and inhibitory interneurons in the rat gustatory cortex.* Cereb Cortex, 2011. **21**(3): p. 597-606.
121. Vincis, R. and A. Fontanini, *A gustocentric perspective to understanding primary sensory cortices.* Curr Opin Neurobiol, 2016. **40**: p. 118-124.
122. Sreenivasan, V., et al., *Parallel pathways from motor and somatosensory cortex for controlling whisker movements in mice.* Eur J Neurosci, 2015. **41**(3): p. 354-67.
123. Avermann, M., et al., *Microcircuits of excitatory and inhibitory neurons in layer 2/3 of mouse barrel cortex.* J Neurophysiol, 2012. **107**(11): p. 3116-34.
124. Linster, C. and A. Fontanini, *Functional neuromodulation of chemosensation in vertebrates.* Curr Opin Neurobiol, 2014. **29**: p. 82-7.

125. Gutierrez, R., et al., *Orbitofrontal ensemble activity monitors licking and distinguishes among natural rewards.* J Neurophysiol, 2006. **95**(1): p. 119-33.
126. Kloc, M. and A. Maffei, *Target-specific properties of thalamocortical synapses onto layer 4 of mouse primary visual cortex.* J Neurosci, 2014. **34**(46): p. 15455-65.
127. Cohen, J.Y., et al., *Neuron-type-specific signals for reward and punishment in the ventral tegmental area.* Nature, 2012. **482**(7383): p. 85-8.
128. Gallistel, C.R., S. Fairhurst, and P. Balsam, *The learning curve: implications of a quantitative analysis.* Proc Natl Acad Sci U S A, 2004. **101**(36): p. 13124-31.